Matter

CellPress

Article

Inhalable dry powder mRNA vaccines based on extracellular vesicles

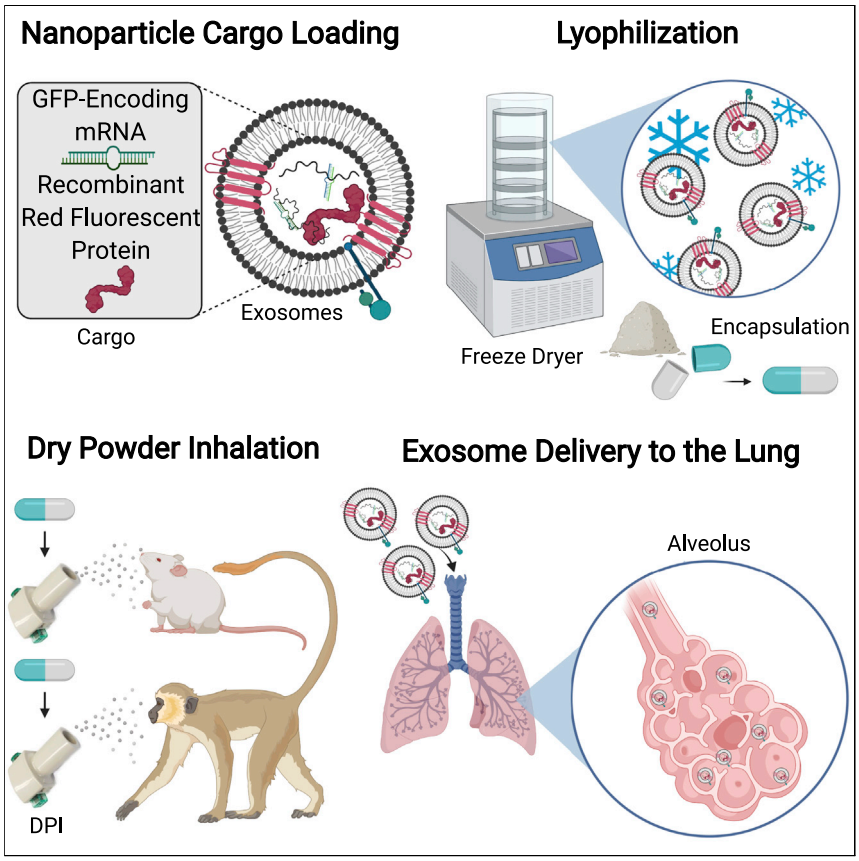

Lipid nanoparticles have limitations in inhaled drug delivery, including low pulmonary bioavailability and unoptimized formulation. Lung-derived extracellular vesicles (Lung-Exos) may be naturally equipped for drug delivery to the lung. We determined the biodistribution of Lung-Exos following nebulization and dry powder inhalation, where Lung-Exos outperformed their biological and synthetic nanoparticle counterparts in drug distribution and retention. As an inhalable vaccine, Lung-Exos elicited greater protective antibody responses and pseudoviral clearance than their synthetic counterpart.

Kristen D. Popowski, Adele Moatti, Grant Scull, ..., Alon Greenbaum, Phuong-Uyen C. Dinh, Ke Cheng

pcdinh@ncsu.edu (P.-U.C.D.)
ke_cheng@ncsu.edu (K.C.)

Highlights

Lung extracellular vesicles (Lung-Exos) can package mRNA and protein drugs

Lung-Exos are deliverable through nebulization and dry powder inhalation

Dry powder Lung-Exos are room-temperature stable up to 28 days

Drug-loaded Lung-Exos can serve as an inhalable vaccine to illicit immune responses

6 **Development**
Practical, real world, technological considerations and constraints

Popowski et al., Matter 5, 2960–2974
September 7, 2022
https://doi.org/10.1016/j.matt.2022.06.012

CellPress

Matter

Article

Inhalable dry powder mRNA vaccines based on extracellular vesicles

Kristen D. Popowski,[1,2] Adele Moatti,[2,3] Grant Scull,[2,3] Dylan Silkstone,[2,3] Halle Lutz,[1,2] Blanca López de Juan Abad,[1] Arianna George,[4,5] Elizabeth Belcher,[3] Dashuai Zhu,[1,2] Xuan Mei,[1,2,3] Xiao Cheng,[1,3] Megan Cislo,[5,6] Asma Ghodsi,[1] Yuheng Cai,[2,3] Ke Huang,[1,2,3] Junlang Li,[1,3] Ashley C. Brown,[2,3] Alon Greenbaum,[2,3] Phuong-Uyen C. Dinh,[1,2,*] and Ke Cheng[1,2,3,7,8,*]

SUMMARY

Respiratory diseases are a global burden, with millions of deaths attributed to pulmonary illnesses and dysfunctions. Therapeutics have been developed, but they present major limitations regarding pulmonary bioavailability and product stability. To circumvent such limitations, we developed room-temperature-stable inhalable lung-derived extracellular vesicles or exosomes (Lung-Exos) as mRNA and protein drug carriers. Compared with standard synthetic nanoparticle liposomes (Lipos), Lung-Exos exhibited superior distribution to the bronchioles and parenchyma and are deliverable to the lungs of rodents and nonhuman primates (NHPs) by dry powder inhalation. In a vaccine application, severe acute respiratory coronavirus 2 (SARS-CoV-2) spike (S) protein encoding mRNA-loaded Lung-Exos (S-Exos) elicited greater immunoglobulin G (IgG) and secretory IgA (SIgA) responses than its loaded liposome (S-Lipo) counterpart. Importantly, S-Exos remained functional at room-temperature storage for one month. Our results suggest that extracellular vesicles can serve as an inhaled mRNA drug-delivery system that is superior to synthetic liposomes.

INTRODUCTION

Respiratory diseases are among the leading causes of morbidity and mortality worldwide,[1] with coronavirus disease 2019 (COVID-19)[2] remaining prevalent in the ongoing pandemic. A wide range of therapeutics have been developed and repurposed to treat respiratory diseases, including small-molecule drugs,[3,4] stem cells[5–9] and their derivatives,[10–13] and, notably, messenger RNA (mRNA)[14–17] and protein vaccines.[18,19] Currently, three intramuscular (IM) vaccines (Pfizer-BioNTech, Moderna, and Janssen) have been authorized for COVID-19 by the US Food and Drug Administration. However, formulating drugs and vaccines for inhaled delivery may improve their efficacy and bioavailability in the lung as well as improve patient compliance.

Although inhalation delivery is attractive due to its local, noninvasive, and highly absorptive properties, drug formulation with optimized physiochemical parameters remains the key obstacle.[20] A possible solution is colloidal drug-delivery systems, which help overcome poor drug solubility and hydrophobicity by providing protection through nanoparticle encapsulation.[21] Plus, nanoparticles retained in the lung prolong drug release in the highly vascularized pulmonary and bronchial circulations.[22] Lipid nanoparticles (LNPs) have been successful as drug-delivery vesicles

PROGRESS AND POTENTIAL STATEMENT

Research in extracellular vesicles (EVs) is important to the field of translational medicine to develop therapeutics that are limited by poor cellular targeting and efficacy. The biological composition of EVs can be exploited as drug-delivery vehicles that may be engineered for cellular targeting or eliciting specific immune responses through their functions in membrane trafficking and cellular signaling. With the molecular composition of EVs varying depending on their parent-cell origin, the derivation of EVs can further refine nanomedicine by utilizing nanoparticles that are recognized by specific cellular microenvironments. EVs are found in almost all biological fluids, opening the application of EVs as tailored drug-delivery vesicles to a wide range of diseases.

for vaccines, most notably in the liposome-encapsulated COVID-19 mRNA IM vaccines.[23] However, major limitations such as deep-freezing storage and healthcare professional administration have led to the expansion of the LNP platform to alternative delivery routes such as self-administered inhalation. In addition, the lung has sophisticated pulmonary defense mechanisms and surfactants that protect it against inhaled particulates and microbes.[22,24] Therefore, the formulation of nanoparticle drug-delivery systems must be optimized to overcome these inherent obstacles.

Exosomes, biologically derived nanoparticles, may be naturally equipped to withstand pulmonary conditions. They are nanosized extracellular vesicles secreted by numerous cell types and found in almost all biological fluids.[25] Initially regarded as cellular debris, exosomes are now understood to have potent roles in autocrine and paracrine signaling.[26–28] Originating from the endosomal system and shedding from the plasma membrane, exosomes contain various cocktails of RNA, protein, and lipid cargo with unique parent-cell signatures.[29,30] Lung-derived exosomes can be utilized as sophisticated drug-delivery systems that offer cargo components and membrane features tailored to the lung microenvironment.[20,31] Our group has demonstrated the lung regenerative abilities of human lung spheroid cells (LSCs)[8,9] in rodent models of idiopathic pulmonary fibrosis (IPF), and their safety and efficacy are being tested in a human clinical trial (HALT-IPF, ClinicialTrials.gov: NCT04262167). LSCs and their secreted exosomes (lung-derived extracellular vesicles [Lung-Exos]) have regenerative abilities in IPF models[13] and protective abilities against COVID-19 as decoys.[32] In both disease models, Lung-Exos maintained therapeutic efficacy through jet-nebulization administration, demonstrating the ability of Lung-Exos to function as an inhalable drug-delivery and vaccine vehicle. Additionally, exosomes can be synthetically supplemented to enhance cellular targeting and therapeutic efficacy.[33–35] For example, anti-inflammatory peptides[36] can be linked onto the exosomal membrane, engineering an immune cell targeting nanomedicine. The combination of vesicle derivation and supplementation allows for a customizable nanoparticle delivery platform that can be utilized across many lung diseases.

Although exosomes as inhaled therapeutics and RNA delivery vehicles have been demonstrated,[13,37] the distribution and retention of exosome particles in the lung have yet to be determined. Drug effectiveness depends on proper deposition of particles within the respirable fraction, requiring optimized nanoparticle formulation. In this study, we sought to elucidate the biodistribution of lung-derived exosomes upon nebulization, baselined to liposomes (Lipos) as a commercial standard. Furthermore, to provide a room-temperature-stable product, we formulated exosomes as a lyophilized dry powder to investigate their stability and inhaled biodistribution in the lung of both the mouse and African green monkey (AGM). The parent-cell signature of Lung-Exos may suggest that they are naturally optimized for the distribution and retention within the lung, which may allow them to bypass pulmonary clearance more efficiently than Lipos or exosomes derived from other cell types. Through this enhanced pulmonary bioavailability, we hypothesize that lung-derived exosomes elicit greater therapeutic responses for pulmonary diseases and serve as a customizable drug-delivery vehicle for room-temperature-stable inhaled mRNA therapeutics.

RESULTS

Exosome distribution in the bronchioles and parenchyma are superior to that of synthetic nanoparticles

Red fluorescent protein (RFP)-labeled lung-derived exosomes (RFP-Exos) and Lipos (RFP-Lipos) were fabricated to generate trackable nanoparticles for biodistribution

[1]Department of Molecular Biomedical Sciences, North Carolina State University, Raleigh, NC 27607, USA

[2]Comparative Medicine Institute, North Carolina State University, Raleigh, NC 27607, USA

[3]Joint Department of Biomedical Engineering, University of North Carolina at Chapel Hill and North Carolina State University, Raleigh/Chapel Hill, NC 27607/27599, USA

[4]Department of Molecular and Structural Biochemistry, North Carolina State University, Raleigh, NC 27695, USA

[5]Department of Biological Sciences, North Carolina State University, Raleigh, NC 27695, USA

[6]Department of Food, Bioprocessing, and Nutrition Sciences, North Carolina State University, Raleigh, NC 27695, USA

[7]Division of Pharmacoengineering and Molecular Pharmaceutics, University of North Carolina at Chapel Hill, Chapel Hill, NC 27599, USA

[8]Lead contact

*Correspondence: pcdinh@ncsu.edu (P.-U.C.D.), ke_cheng@ncsu.edu (K.C.)

https://doi.org/10.1016/j.matt.2022.06.012

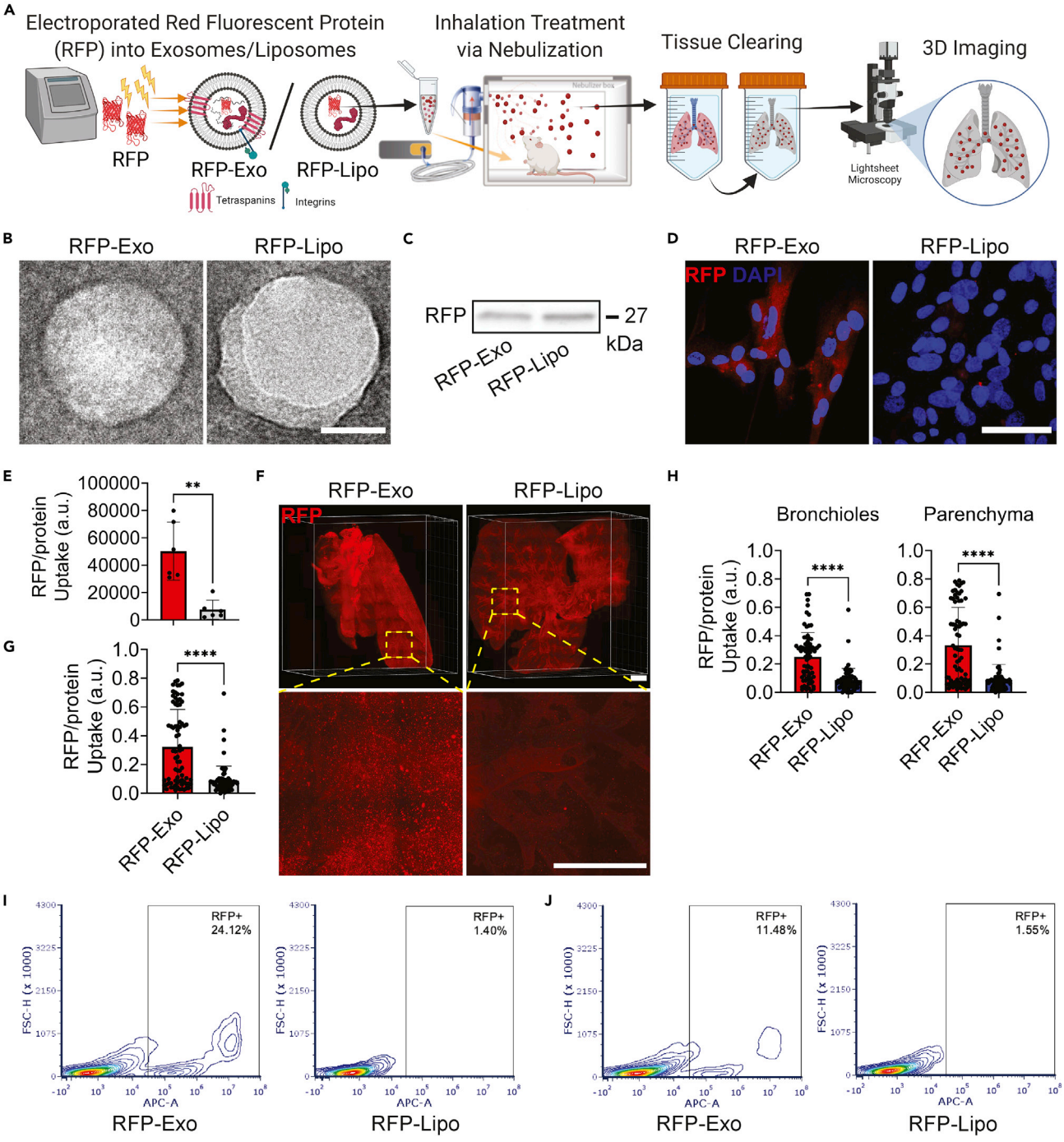

Figure 1. Fabrication and distribution of exosomes and liposomes

(A) Schematic showing protein loading into lung-derived exosomes (RFP-Exos) and liposomes (RFP-Lipos), nebulization administration, *ex vivo* lung-tissue clearing, and 3D imaging by LSFM. Created with BioRender.com.

(B) TEM images of RFP-Exos and RFP-Lipos; scale bar: 50 nm.

(C) Immunoblot of RFP in exosome and liposome lysate.

(D) Representative immunostaining images of lung parenchymal cells for RFP (red) and DAPI (blue); scale bar: 50 μm.

(E) Quantification of RFP-Exo and RFP-Lipo pixel intensity normalized to nuclei in lung parenchymal cell images; n = 6 per group; data are represented as mean ± standard deviation.

(F) LSFM images of cleared mouse lungs after RFP-Exo and RFP-Lipo nebulization; scale bar: 1,000 μm.

Figure 1. *Continued*
(G) Quantification of the integrated density of RFP normalized to the whole-lung area; n = 74 total slices from two biological replicates per group; data are represented as mean ± standard deviation.
(H) Quantification of the integrated density of RFP normalized to segmented bronchiole and parenchymal regions from whole-lung images; n = 74 total slices from two biological replicates per group; data are represented as mean ± standard deviation.
(I and J) Flow cytometry analysis of lung parenchymal cells co-cultured with RFP-Exos or RFP-Lipos (I) and murine lung cells that received nebulized RFP-Exos or RFP-Lipos (J).

analysis in the murine lung after inhalation treatment through three-dimensional (3D) imaging (Figure 1A). The nanoparticles were characterized by transmission electron microscopy (TEM), confirming that the isolation of exosomes and Lipos did not disrupt vesicular membrane integrity (Figure 1B). RFP loading was verified by immunoblotting (Figure 1C). When co-cultured with lung parenchymal cells, RFP-Exo had a 6.7-fold increase in cellular uptake and RFP protein expression compared with cells cultured with RFP-Lipo (Figures 1D and 1E). Next, the biodistribution of nanoparticles *in vivo* were evaluated through light-sheet fluorescence microscopy (LSFM) (Figure 1F). Healthy mice received a single dose of RFP-Exos or RFP-Lipos via nebulization and were sacrificed after 24 h. LSFM imaging confirmed nanoparticle delivery to the conducting airways and the deep lung, with an accumulation of RFP-Exos in the upper pulmonary regions (Videos S1 and S2). Quantification of nanoparticle delivery to the whole lung demonstrated a 3.7-fold improvement in RFP-Exo retention and uptake compared with RFP-Lipo (Figure 1G). Segmentation of the lung into bronchial and parenchymal regions revealed 2.9- and 3.8-fold improvements in RFP-Exo retention and uptake, respectively, compared with RFP-Lipo (Figure 1H). Flow cytometry analysis in lung parenchymal cells (Figure 1I) and in the murine lung following nebulization (Figure 1J) confirmed greater cellular uptake of RFP-Exos than RFP-Lipos. The drug-loading capabilities of lung-derived exosomes (Lung-Exos and Lipos were expanded by loading GFP-encoding mRNA to evaluate nanoparticle mRNA uptake. Lung parenchymal cells that received GFP-Exos demonstrated more rapid internalization of exosomal mRNA than liposomal mRNA (Figure S1). These data confirm that our nanoparticle labeling system maintains nanoparticle integrity while delivering functional and translatable cargo after jet nebulization. *In vitro* and *in vivo* analyses suggest superior retention and cellular uptake of exosomes over Lipos in the lung. The native lung signature of lung-derived exosomes may enhance pulmonary bioavailability, resulting in an optimized nanoparticle vesicle for drug delivery for respiratory diseases.

Lung-derived exosomes efficiently penetrate mucus

Delivery of inhaled therapeutics must penetrate the lung's protective mucus lining to provide pulmonary bioavailability. Lung-Exos were compared against human embryonic kidney (HEK)-derived exosomes (HEK-Exos) and Lipos to determine if nanoparticle derivation affected mucus penetrance. To test this, we used a model of the human airway at the air-liquid interface (Figure S2A), with human mucus-secreting bronchial epithelial cells lining the transwell membrane and human lung parenchymal cells lining the well (Figure S2B). Immunostaining confirmed the mucus lining in the transwell membrane and delivery of DiD-labeled nanoparticles (Figure S2C). Quantification of nanoparticle penetrance into the wells revealed the greatest uptake of Lung-Exos (Figure S2D), with the highest percentage of cellular uptake by lung parenchymal cells (Figure S2E) by 24 h. Likewise, Lung-Exos had the least entrapment by the mucus-lined membrane (Figure S2F) and the lowest percentage of cellular uptake by bronchial epithelial cells (Figure S2G). These data confirm mucus penetrance of the nanoparticles and suggest that Lung-Exos can most efficiently evade mucoadhesion, overcoming the lung's natural defense mechanism and allowing for greater parenchymal bioavailability.

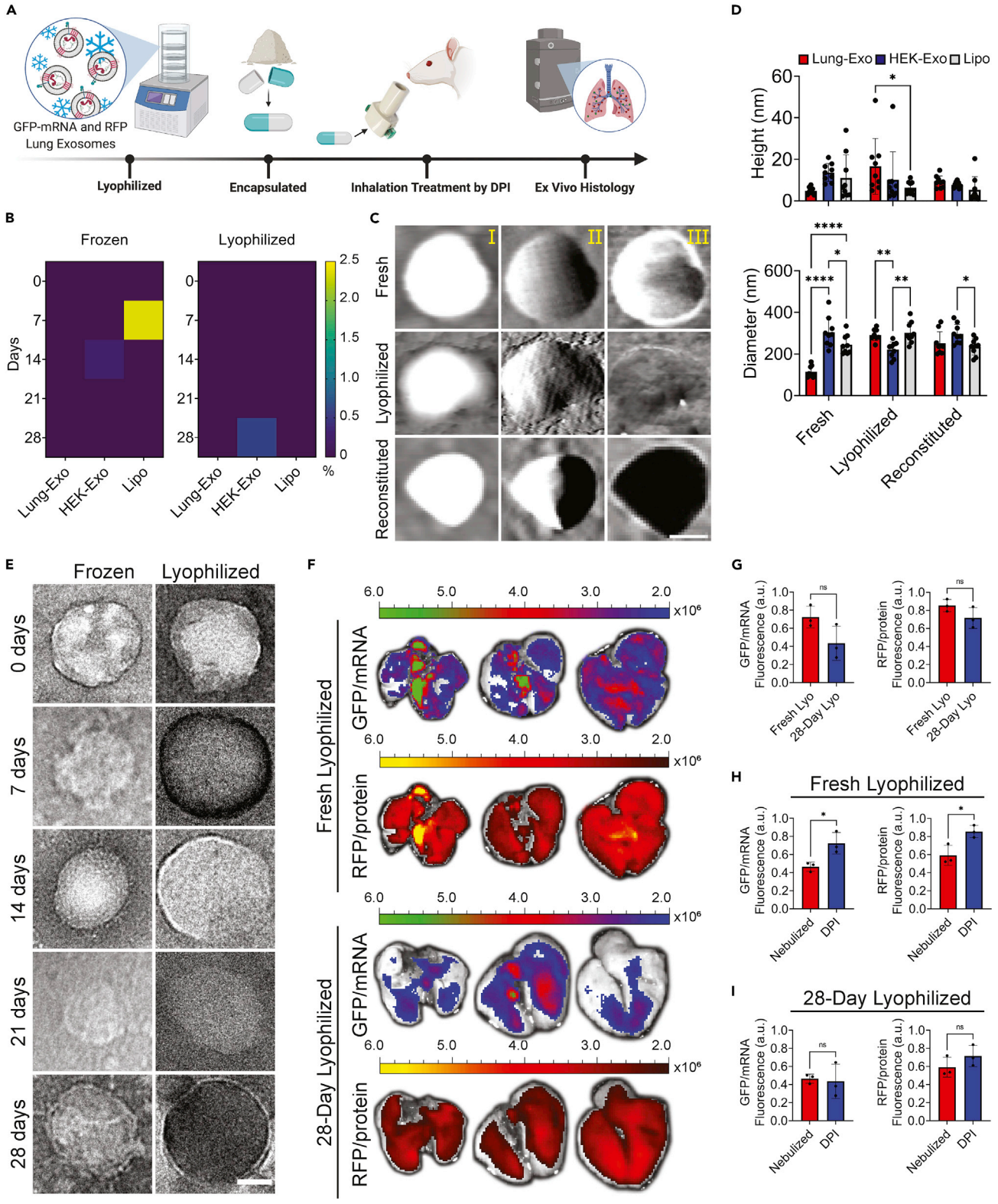

Figure 2. Stability and distribution of lung-derived exosomes in dry powder formulation in the murine lung

(A) Schematic of mRNA and protein-loaded lung-derived exosome lyophilization, encapsulation, rodent DPI administration, and *ex vivo* histology. Created with BioRender.com.

Figure 2. *Continued*

(B) Heatmaps of RFP leakage from Lung-Exos, HEK-Exos, and Lipos detected by ELISA; n = 2 per group.

(C) Representative AFM height (I), amplitude (II), and phase (III) images of Lung-Exos; scale bar: 50 nm.

(D) Quantification of the height and diameter of Lung-Exos, HEK-Exos, and Lipos from AFM images; n = 9 per group; data are represented as mean ± standard deviation.

(E) TEM images of Lung-Exos at frozen (Frozen) or room (Lyophilized) temperatures; scale bar: 50 nm.

(F) *Ex vivo* images of mouse lungs that received fresh lyophilized (0 days) and 28-day-old lyophilized Lung-Exos via dry powder inhalation after 24 h.

(G) Quantification of the integrated density of GFP and RFP fluorescence in *ex vivo* mouse lungs 24 h after fresh (Fresh-Lyos) and 28-day-old (28-Day Lyos) dry powder inhalation; n = 3 per group; data are represented as mean ± standard deviation.

(H) Quantification of the integrated density of GFP and RFP fluorescence in *ex vivo* mouse lungs 24 h after nebulization and fresh (Fresh-Lyos) dry powder inhalation; n = 3 per group; data are represented as mean ± standard deviation.

(I) Quantification of the integrated density of GFP and RFP fluorescence in *ex vivo* mouse lungs 24 h after nebulization and 28-day-old (28-Day Lyos) dry powder inhalation; n = 3 per group; data are represented as mean ± standard deviation.

Lung-derived exosomes are room-temperature stable and distributable in dry powder formulation in the murine lung

Room-temperature formulation of therapeutics circumvents major limitations in traditional IM vaccine delivery: deep-freezing storage, healthcare professional administration, and reduced patient compliance. Therefore, we reformulated our liquid nanoparticle suspensions into dry, lyophilized powder for dry powder inhalation (DPI) administration. We verified the efficacy and stability of room-temperature lyophilized Lung-Exos up to 28 days in the murine lung (Figure 2A). To verify dry powder nanoparticle stability and shelf life, lyophilized nanoparticle cargo leakage was tested by an enzyme-linked immunosorbent assay (ELISA), where nanoparticles had less than 2.4% of total pg/mL cargo leakage at day 28 of room-temperature storage (Figures 2B and S3). Next, the morphology of nanoparticles was evaluated across their fresh and lyophilized formulations, as well as lyophilized powder reconstituted in water (reconstituted), to mimic rehydration of dry powder by saliva and mucus. TEM (Figures 2E and S4) and atomic force microscopy (AFM) verified that reformulation and rehydration did not affect nanoparticle membrane integrity (Figures 2C and S5) but did affect size distributions through clumping (Figure S6–S8). Lyophilization increased nanoparticle height and diameter (Figure 2D) but remained as small respiratory droplets upon reconstitution. Across all formulations, the nanoparticle diameters are approximately 10-fold larger, which may be explained by tip dilation[38] that reports larger lateral dimensions than 2D analysis such as through TEM.[39] Cross-section measurement curves demonstrate a restoration of membrane "smoothness" in reconstituted nanoparticles, mimicking fresh formulation (Figure S9). Next, we delivered the lyophilized Lung-Exos via DPI, where *ex vivo* images (Figure 2F) of mouse lungs who received fresh (fresh lyophilized) and 28-day-old (28-day lyophilized) dry powder Lung-Exos had no significant difference in exosomal mRNA and protein distribution (Figure 2G). mRNA activity showed greater variability at it 28-day-old state, but protein activity remained more stable.

Compared with nebulized exosome biodistribution, both fresh (Figure 2H) and 28-day-old (Figure 2I) lyophilized exosomes have trends of greater pulmonary distribution 24 h after administration. Lyophilized Lung-Exo is a room-temperature-stable exosome formulation that can deliver functional and translatable cargo via DPI.

Distribution of exosomes via DPI in AGMs

Dry powder inhalers offer an at-home or on-the-go electronic-free administration of therapeutics through a user-friendly device designed specifically for pulmonary disease treatment, providing local drug delivery and reducing side effects associated with IM and oral drugs. Lung-Exos, HEK-Exos, and Lipos were lyophilized and encapsulated into commercially available hydroxypropyl methylcellulose (HPMC) capsules, and particle-distribution analysis was performed on DPIs with a

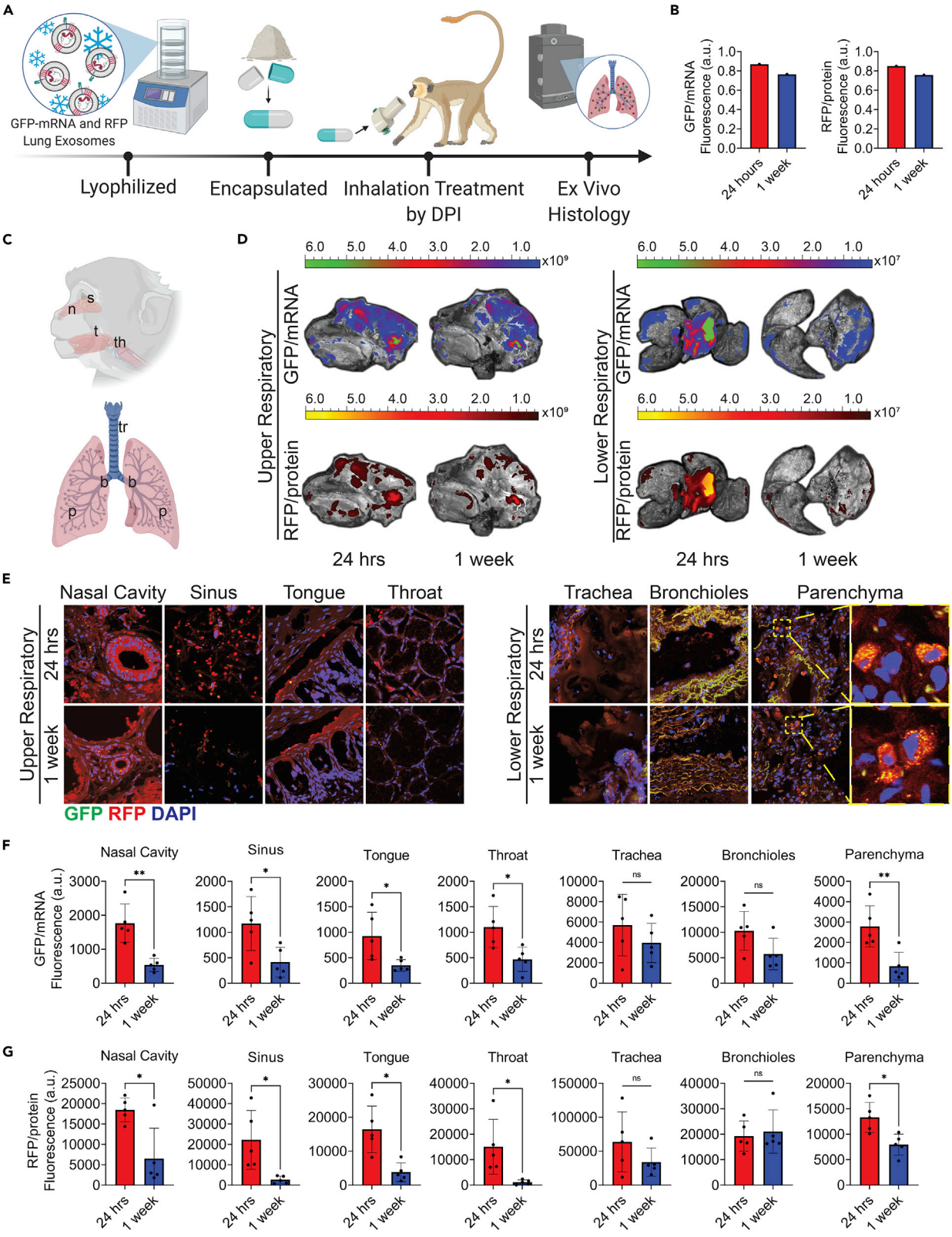
A
GFP-mRNA and RFP
Lung Exosomes
Lyophilized
Encapsulated
Inhalation Treatment
by DPI
Ex Vivo
Histology
B
GFP/mRNA
Fluorescence (a.u.)
RFP/protein
Fluorescence (a.u.)
24 hours
1 week
C
s
n
t
th
tr
b
b
p
p
D
Upper Respiratory
Lower Respiratory
GFP/mRNA
RFP/protein
x10⁹
x10⁷
24 hrs
1 week
E
Nasal Cavity
Sinus
Tongue
Throat
Trachea
Bronchioles
Parenchyma
Upper Respiratory
Lower Respiratory
24 hrs
1 week
GFP RFP DAPI
F
GFP/mRNA
Fluorescence (a.u.)
G
RFP/protein
Fluorescence (a.u.)

Figure 3. Distribution of lung-derived exosomes via dry powder inhalation in African green monkeys

(A) Schematic of mRNA and protein-loaded lung-derived exosome lyophilization, encapsulation, non-human primate DPI administration, and *ex vivo* histology. Created with BioRender.com.

(B) Quantification of the integrated density of GFP and RFP fluorescence in *ex vivo* primate lungs 24 h and 1 week after dry powder inhalation; n = 1 per group.

(C) Schematic showing upper respiratory tissue sectioning for nasal (n), sinus (s), tongue (t), and throat (th) sections and lower respiratory tissue sectioning for tracheal (tr), bronchial (b), and parenchymal (p) sections. Created with BioRender.com.

(D) *Ex vivo* images of primate head cross-sections and lungs 24 h and 1 week after lyophilized Lung-Exos via dry powder inhalation.

(E) Representative immunostaining images of nasal cavity, sinus, tongue, throat, trachea, bronchioles, and parenchyma sections for GFP (green), RFP (red), and DAPI (blue); scale bar: 100 μm in representative images; scale bar: 1 μm in parenchyma sections.

(F) Quantification of Lung-Exo GFP pixel intensity normalized to nuclei in nasal cavity, sinus, tongue, throat, trachea, bronchioles, and parenchyma sections; n = 5 per group; data are represented as mean ± standard deviation.

(G) Quantification of Lung-Exo RFP pixel intensity normalized to nuclei in nasal cavity, sinus, tongue, throat, trachea, bronchioles, and parenchyma sections; n = 5 per group; data are represented as mean ± standard deviation.

range of resistances from low to ultra high. A commercially available RS01 high-resistance DPI was selected for its overall greater output of aerosols within the respirable fraction (Figure S10)[40] and consistent particle distributions across the nanoparticles (Figure S11). Using this DPI, we tracked exosome biodistribution in the AGM by delivering a single dose of lyophilized Lung-Exos and sacrificing after 24 h and 1 week for further analysis (Figure 3A). AGMs receiving Lung-Exos were compared against a negative control AGM to evaluate autofluorescence. *Ex vivo* imaging revealed a similar biodistribution of exosomal mRNA and protein cargo throughout the lung (Figures 3B and 3D). Lung-Exos were maintained in the lung 1 week after administration (Figures 3B and 3D). Further immunostaining analysis of the upper and lower respiratory tracts confirmed exosome delivery (Figures 3C, 3E, and S12) and the greatest nanoparticle deposition into the lung (Figure S13). Exosomal mRNA (Figure 3F) and protein (Figure 3G) were significantly cleared from the upper respiratory and parenchymal regions after 1 week. Tracheal and bronchial regions maintained similar GFP and RFP fluorescence, which may be attributed to by the autofluorescent nature of airway tissue due to collagen, particularly in the fluorescein isothiocyanate (FITC) range (Figure S13).[41,42] Collagen fibers in the trachea and bronchioles are highly fluorescent in both the exosome-treated (Figure S12) and control (Figure S14) tissue sections and do not reflect exosomal mRNA and protein deposition. Overall, Lung-Exos are distributable in the simian upper and lower respiratory tracts through DPI.

SARS-CoV-2 spike-loaded exosomes elicit antibody protection through DPI

In our final study, the therapeutic potential of lyophilized Lung-Exos was tested as an inhaled vaccine against COVID-19. mRNA encoding the severe acute respiratory coronavirus 2 (SARS-CoV-2) spike (S) protein was loaded into Lung-Exos and Lipos and formulated for DPI, generating S-Exos and S-Lipos, respectively (Figure 4A). Although not naturally immunogenic, exosomes can be supplemented with agents such as mRNA to activate specific immune responses.[43] To confirm long-term storage efficiency, S-Exos and S-Lipos were stored for 1 month at room temperature prior to characterization and mouse vaccination. Nanoparticle vaccine integrity was verified by TEM (Figure 4B) and nanoparticle-tracking analysis (NTA) (Figures 4C and 4D). S-protein-encoding mRNA loading and *in vitro* cellular translation were verified by immunoblotting (Figure 4E), where S-Exos and S-Lipos had similar results (Figure 3F). Our inhaled vaccine was then tested in healthy mice, which received two doses of S-Exos or S-Lipos via DPI. The mice were sacrificed 1 week after the second dose, and bronchoalveolar lavage fluid (BALF) and nasopharyngeal lavage fluid (NPLF) were collected to assess anti-S immunoglobulin G (IgG) and secretory IgA (SIgA) antibody production, respectively (Figure 4A). ELISAs revealed that both S-Exos and S-Lipos produced

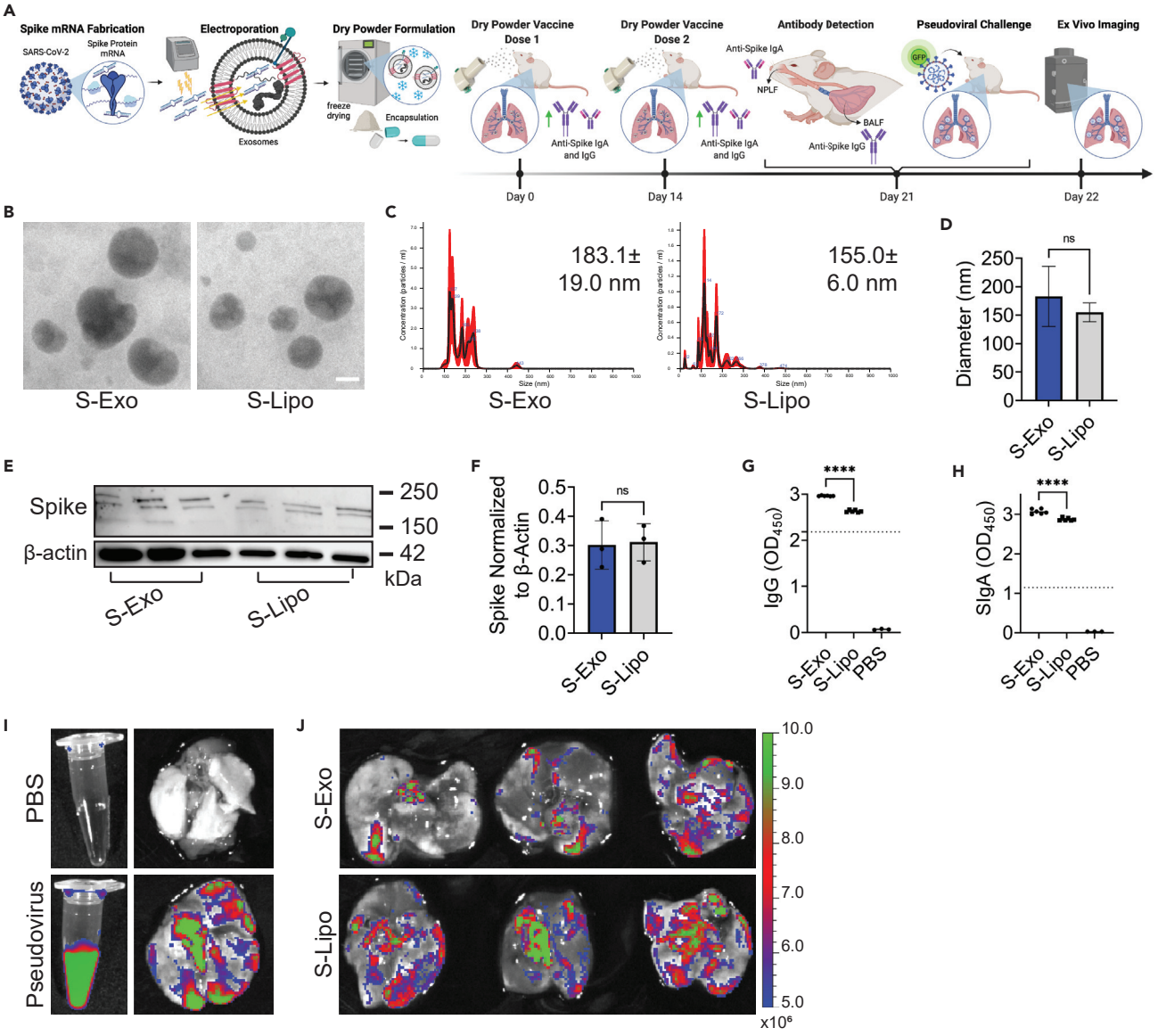

Figure 4. Dry powder inhalation of S-protein-loaded lung-derived exosomes elicit greater immune responses than their synthetic counterpart

(A) Schematic of S protein mRNA loading into lung-derived exosomes, dry powder formulation, inhaled vaccine delivery doses, antibody production against SARS-CoV-2 spike protein, and pseudoviral challenge. Created with BioRender.com.

(B) TEM images of S-Exos and S-Lipos at room temperature; scale bar: 50 nm.

(C) NTA size-distribution analysis.

(D) Quantification of NTA size-distribution analysis of the average mean ± standard error of five replicates; n = 1 per group.

(E) Immunoblots of S protein in mouse lung lysate.

(F) Quantification of immunoblots normalized to β-actin; n = 3 per group; data are represented as mean ± standard deviation.

(G) Anti-spike IgG antibody titer from murine BALF detected by ELISA; n = 6 per group; data are represented as mean ± standard deviation.

(H) Anti-spike SIgA antibody titer from murine NPLF detected by ELISA; n = 6 per group; data are represented as mean ± standard deviation.

(I) *Ex vivo* images of PBS or pseudovirus in solution (left) and in lungs 24 h after dry powder inhalation (right).

(J) *Ex vivo* images of S-Exo- or S-Lipo-vaccinated lungs 24 h after pseudoviral challenge.

sufficient IgG (>2.18325; Figure 4G) and SIgA (>1.14595; Figure 4H) antibodies to induce neutralizing antibody responses. However, DPI of S-Exos produced significantly higher amounts of antibodies than S-Lipos (Figures 4G and 4H). This suggests that S-Exos would have superior protection against SARS-CoV-2 infection over S-Lipos as an inhaled vaccine. Coupled with enhanced mucus

penetrance, S-Exos may further facilitate passive IgG diffusion into the pulmonary epithelial lining fluid.[44] To assess the ability to clear inhaled pseudovirus, mice vaccinated with two doses of S-Exos or S-Lipos were challenged with wild-type SARS-CoV-2 pseudoviral particles with a GFP reporter (Figure 4I). Twenty-four h after pseudoviral challenge, mice vaccinated with S-Exos showed significantly greater viral clearance than their S-Lipo counterpart (Figure 4J), suggesting that S-Exos would provide more rapid protection against viral infection. The features of Lung-Exos have significant advantages over their synthetic nanoparticle counterpart, suggesting that exosomes contain additional therapeutic benefits regarding pulmonary targeting, retention, and immune responses. Biological nanoparticles such as exosomes can be exploited as inhaled drug-delivery vehicles to maximize drug targeting, delivery, and therapeutic efficacy.

DISCUSSION

Altogether, we have demonstrated the formulation and biodistribution of inhaled exosomes and Lipos in mouse and nonhuman primate (NHP) lungs. Exosomal and liposomal mRNA and protein cargo are stable and maintain biological function upon dry powder formulation and DPI, with a shelf life extending 28 days. We showed that lung-derived exosomes most efficiently evade mucoadhesion while maintaining higher exosomal mRNA and protein cargo deposition, retention, and distribution in lung than their Lipo counterpart. Lung-derived exosomes had the highest nanoparticle delivery to the bronchioles and parenchyma, suggesting that nanoparticle phenotypes that are native to the lung microenvironment have enhanced cellular targeting and bioavailability within the lung.

For the first time, we showed that dry powder formulation of lung-derived exosomes is room-temperature stable and is compatible with a clinically used DPI device for at-home administration. The *chlorocebus sabaeus* NHP model most closely replicates the human airway and respiratory physiology, and exosome delivery was verified in the upper and lower respiratory tracts through DPI administration. Lung-derived exosomes were retained in the primate lung 1 week after a single DPI dose, delivering functional mRNA and protein exosomal cargo to the nose and to the deep lung. Lung-derived exosomes are functional as an inhaled therapeutic and drug-delivery vesicle for both upper and lower respiratory diseases.

Additionally, lung-derived exosomes have enhanced efficacy for pulmonary disease applications. S-protein-encoding mRNA remains effective in exosomes after 1 month of room temperature storage when lyophilized. As an inhaled vaccine, S-protein-loaded lung-derived exosomes elicited stronger immune responses than their synthetic counterpart, emphasizing the immunological advantages of biological nanoparticles for inhaled vaccines. Mice vaccinated with S-protein-loaded exosomes were able to more rapidly clear pseudoviral infection than Lipos, further emphasizing the enhanced efficacy of exosomes. Lung-derived exosomes offer a unique room-temperature-stable nanoparticle drug-delivery system, with enhanced bioavailability, that can serve as an mRNA and protein drug-delivery vesicle tailored for lung diseases.

EXPERIMENTAL PROCEDURES

Resource availability

Lead contact

Further information and requests for resources and reagents should be directed to and will be fulfilled by the lead contact, Ke Cheng (ke_cheng@ncsu.edu).

Materials availability

All unique/stable reagents generated in this study are available from the lead contact with a completed materials transfer agreement.

Data and code availability

All data reported in this paper will be shared by the lead contact upon request. This paper does not report original code. Any additional information required to reanalyze the data reported in this paper is available from the lead contact upon request.

Cell culture

Human LSCs were generated from healthy whole-lung samples from the Cystic Fibrosis and Pulmonary Diseases Research and Treatment Center at the University of North Carolina at Chapel Hill and expanded as previously described.[7,8,45] LSCs were plated on a fibronectin-coated (Corning, Corning, NY, USA) flask and maintained in Iscove's modified Dulbecco's media (IMDM; Thermo Fisher Scientific, Waltham, MA, USA) containing 20% fetal bovine serum (FBS; Corning), 1% L-glutamine (Thermo Fisher Scientific), 0.5% Gentamicin (Thermo Fisher Scientific), and 0.18% 2-mercaptoethanol (Thermo Fisher Scientific). HEK 293T cells were purchased from American Type Culture Collection (ATCC; American Type Culture Collection, Manassas, VA, USA). HEK cells were plated on a flask and maintained in minimum essential media (MEM; Thermo Fisher Scientific) containing 10% FBS, 1% L-glutamine, 0.5% Gentamicin, and 0.18% 2-mercaptoethanol. Human bronchial epithelial cells were purchased from Lonza (CC-2540B; Lonza, Basel, Switzerland) and maintained according to manufacturer's instructions. Media changes on all cultures were performed every other day. LSCs and HEK cells were allowed to reach 70%–80% confluence before generating serum-free secretome (Lung-Secretome, HEK-Secretome), as previously described.[13] Lung- and HEK-Secretome were collected and filtered through a 0.22-μm filter to remove cellular debris. All procedures performed in this study involving human samples were in accordance with the ethical standards of the institutional research committee and with the guidelines set by the Declaration of Helsinki.

Exosome isolation and characterization

Lung-Exos and HEK-Exos were collected and isolated from Lung-Secretome and HEK-Secretome using an ultrafiltration method.[46] Filtered secretome was pipetted into a 100-kDa Amicon centrifugal filter unit (MilliporeSigma, Burlington, MA, USA) and centrifuged at 400 RCF and 10°C. After all media passed through the centrifugal filter unit, remaining exosomes were detached from the filter and resuspended using 1X Dulbecco's phosphate-buffered saline (DPBS; Thermo Fisher Scientific) with 25 mM trehalose (MilliporeSigma) for further analysis.[47] Pegylated Remote Loadable Lipos were purchased from Avanti Polar Lipids (Avanti Polar Lipids, Alabaster, AL, USA). LSC-Exos, HEK-Exos, and Lipos were fixed with 4% paraformaldehyde (PFA; Electron Microscopy Sciences, Hatfield, PA, USA) and 1% glutaraldehyde (Sigma-Aldrich, St. Louis, MO, USA) onto 100 mesh copper grids (Electron Microscopy Sciences, Hartfield, PA, USA) for TEM imaging (JEOL JEM-2000FX, Peabody, MA, USA). Samples were stained with Vanadium Negative Stain (ab172780; Abcam, Cambridge, UK). Sample concentrations and mean diameters were quantified by NTA before and after fluorescent label loading (NanoSight NS3000, Malvern Panalytical, Malvern, UK).

Nanoparticle fluorescent label loading

RFP (ab268535; Abcam) was loaded into Lung-Exo and Lipo particles via electroporation, yielding RFP-Exos and RFP-Lipos.[48] One billion nanoparticles from each

sample were diluted in Gene Pulser Electroporation Buffer (Bio-Rad, Hercules, CA, USA) at a 1:9 ratio of nanoparticles to buffer. Ten μg of RFP were added to the nanoparticle-buffer solution and transferred to an ice-cold 0.4 cm Gene Pulser/MicroPulser Electroporation Cuvette (Bio-Rad). The electroporation cuvette was inserted into the Gene Pulser Xcell Total System (Bio-Rad) and electroporated under the following conditions: pulse type: square waveforms; voltage: 200 V; pulse length: 10 ms; number of pulses: 5; pulse interval: 1 s. Electroporation buffer was filtered out of the fluorescently labeled nanoparticles by the ultrafiltration method described above. GFP-encoding mRNA DasherGFP (Aldevron, Fargo, ND, USA) and RFP were loaded into Lung-Exos and Lipos, as described above. Lung-Exos, HEK-Exos, and Lipos were incubated with DiD labeling solution (V22889; Thermo Fisher Scientific) according to the manufacturer's instructions.

Dry powder inhaler formulation and room-temperature stability

Lung-Exos, HEK-Exos, and Lipos were formulated into dry powder through lyophilization (Labconco, Kansas City, MO, USA). The nanoparticles were diluted in DPBS with 25 mM trehalose at a 1:8 ratio of nanoparticle solution volume to DPBS with 25 mM trehalose solution volume. Trehalose solution serves as a cyroprotectant and bulking agent for sufficient powder production.[49] Diluted nanoparticle solutions were stored at -80°C overnight and lyophilized for 24 h. To test the room-temperature stability of lyophilized nanoparticles, RFP-loaded nanoparticles were stored in ambient room conditions for 0, 7, 14, 21, and 28 days. RFP cargo leakage was measured by ELISA (AKR-122; Cell Biolabs, San Diego, CA, USA) per the manufacturer's instructions in non-denatured RFP-loaded nanoparticle solutions. An RFP standard curve was generated using a second-order polynomial model, and cargo-leakage concentrations were interpolated from the standard curve. Percentage of leakage is reported as $\left(\frac{\textit{Interpolated Concentration}}{\textit{Total Loaded RFP Concentration}}\right) \times 100$.

Nanoparticle S protein loading

Full-length DNA sequence of the S surface glycoprotein (SARS-CoV 2 isolate Wuhan-Hu-1, gene ID: 43740568, NC_045512.2:21563-25384) was used to design a plasmid for *in vitro* transcription (IVT). Briefly, a stretch of DNA sequence with two restriction sites, I-CeuI and I-SceI, was cloned into pCR4Blunt-TOPO vector (45-0031; Thermo Fisher Scientific). The full length of the S protein sequence was split to design two gBlocks (Integrated DNA Technologies, Coralville, Iowa, USA), each of which was approximately 1.5- and 2.3-kb long. The T7 promoter sequence (5′-taatacgactcactataggg-3′) was added to the 5′ end of the 1.5-kb gBlock. The two gBlocks were ligated into the backbone vector using I-CeuI, BstEII, and I-SceI. Following sequence confirmation by Sanger sequencing (Genewiz, South Plainfield, NJ, USA), the full-length S protein DNA sequence, cut by I-CeuI and I-SceI, was extracted from TAE agarose gel. IVT was done following the manufacturer's manual of the MEGAscript Kit (AM1333; Thermo Fisher Scientific). High-yield RNA was treated with DNase and cleaned up using the Monarch RNA cleanup kit (T2040L; New England Biolab, Ipswich, MA, USA). Size-confirmed pure IVT S protein mRNA was aliquoted and stored in -80°C until nanoparticle loading. S protein mRNA was loaded into LSC-Exo and Lipo nanoparticles via the electroporation method described above.

Animal procedures

Seven-week-old male CD1 mice (022) were obtained from Charles River Laboratory (Wilmington, MA, USA). RFP-Exos, RFP-Lipos, Lung-Exos, S-Exos, and S-Lipos were administered via jet nebulization (Pari Trek S Portable 459 Compressor Nebulizer

Aerosol System, PARI, Starnberg, Germany) or dry powder inhalation as described above. Fluorescently labeled nanoparticles were given in a single dose of 10^9 particles per kg of body weight. Immediately after sacrifice, the lungs, heart, liver, kidneys, spleen, cecum, and brain were excised and imaged using a Xenogen Live Imager (PerkinElmer, Waltham, MA, USA). Blood was collected in Vacuette ethylenediaminetetraacetic acid (EDTA) tubes (Greiner Bio-One, Kremsmünster, Austria) and centrifuged at maximum speed for 5 min to separate out serum. All animal studies complied with the requirements of the Institutional Animal Care and Use Committee (IACUC) of North Carolina State University.

NHP studies

Three *chlorocebus sabaeus* monkeys were housed at Bioqual. The primates received a single dose of 10^9 lyophilized fluorescently labeled Lung-Exo particles per kg of body weight via DPI. The primates were necropsied 24 h and 1 week after DPI of Lung-Exos. All animal studies complied with the requirements under local, state, and federal regulations and were approved by the Bioqual IACUC.

IgG and SIgA antibody titers

To collect BALF, the trachea was exposed by thoracotomy, and a transverse incision was made at the top of the bronchial bifurcation. A needle was inserted into the trachea to wash the lungs with 200 μL of DPBS. Washing was repeated three times for a total of 600-μL wash fluid. To collect NPLF, the trachea was cut in the middle, and the nasopharynx was washed upwards from the incision with 200 μL DBPS. Washing was repeated three times for a total of 600-μL wash fluid. S-protein-specific IgG (20154; Cell Signaling Technology, Danvers, MA, USA) and SIgA (58873; Cell Signaling Technology) from BALF and NPLF were measured by ELISA per the manufacturer's instructions.

Pseudoviral challenge

Wild-type SARS-CoV-2 pseudoviral particles with a GFP reporter were purchased from Virongy (HaCoV2GFP; Virongy, Manasses, VA, USA). Pseudoviral particles were given in a single dose of 10^9 particles per kg of body weight via DPI, as described above.

Statistical analysis

Statistical analysis was performed using GraphPad Prism analysis software (GraphPad Software, San Diego, CA, USA). Comparisons among two groups were performed using an unpaired t test, followed by Welch's correction test. Comparisons among more than two groups were performed using a parametric one-way ANOVA test followed by Bonferroni's multiple comparisons test. $p \leq 0.05$ was considered statistically significant. The legend is as follows: *$p \leq 0.05$; **$p \leq 0.01$; ***$p \leq 0.001$; ****$p \leq 0.0001$; ns = not significant.

SUPPLEMENTAL INFORMATION

Supplemental information can be found online at https://doi.org/10.1016/j.matt.2022.06.012.

ACKNOWLEDGMENTS

We thank Dr. Jaewook Chung for spike mRNA synthesis, the Analytical Instrumentation Facility at North Carolina State University for TEM imaging, and the North Carolina State University College of Veterinary Medicine Histology Core for histological processing. The nonhuman primate work was performed by Bioqual Inc. This work was supported by grants from the National Institutes of Health (HL123920,

HL137093, HL144002, HL146153, HL147357, and HL149940 to K.C.; HL146701 to A.C.B.; HL164998 to P.-U.C.D.) and the American Heart Association (18TPA34230092 and 19EIA34660286 to K.C.). G.S. is supported by the National Institutes of Health T32GM133393, which is co-directed by K.C.

AUTHOR CONTRIBUTIONS

Conceptualization, P.-U.C.D. and K.C.; methodology, K.D.P., A.M., G.S., D.Z., X.M., X.C., Y.C.; formal analysis, K.D.P.; investigation, K.D.P., A.M., G.S., D.S., H.L., B.L.d.J.A., A. George, E.B., M.C., A. Ghodsi., K.H., and J.L.; resources, A.C.B., A. Greebaum, and K.C.; writing, K.D.P., B.L.d.J.A., and A. George; supervision, P.-U.C.D. and K.C.; funding acquisition, K.C.

DECLARATION OF INTERESTS

North Carolina State University has filed a patent on the technologies related to this study. K.C. is an equity holder and consultant of Xsome Biotech, Inc. Xsome has entered an exclusive license agreement with North Carolina State University.

Received: February 2, 2022
Revised: April 29, 2022
Accepted: June 7, 2022
Published: July 1, 2022

REFERENCES

1. Wisnivesky, J., and De-Torres, J.P. (2019). The global burden of pulmonary diseases: most prevalent problems and opportunities for improvement. Ann. Global Health *85*. https://doi.org/10.5334/aogh.2411.

2. Wang, C., Horby, P.W., Hayden, F.G., and Gao, G.F. (2020). A novel coronavirus outbreak of global health concern. Lancet *395*, 470–473. https://doi.org/10.1016/S0140-6736(20)30185-9.

3. Li, D., Hu, J., Li, D., Yang, W., Yin, S.-F., and Qiu, R. (2021). Reviews on biological activity, clinical trial and synthesis progress of small molecules for the treatment of COVID-19. Top. Curr. Chem. *379*, 4. https://doi.org/10.1007/s41061-020-00318-2.

4. Panoutsopoulos, A.A. (2020). Known drugs and small molecules in the battle for COVID-19 treatment. Genes. Dis. *7*, 528–534. https://doi.org/10.1016/j.gendis.2020.06.007.

5. Cruz, F.F., and Rocco, P.R.M. (2020). The potential of mesenchymal stem cell therapy for chronic lung disease. Expet. Rev. Respir. Med. *14*, 31–39. https://doi.org/10.1080/17476348.2020.1679628.

6. Ji, H.-L., Liu, C., and Zhao, R.-Z. (2020). Stem cell therapy for COVID-19 and other respiratory diseases: global trends of clinical trials. World J. Stem Cell. *12*, 471–480. https://doi.org/10.4252/wjsc.v12.i6.471.

7. Henry, E., Cores, J., Hensley, M.T., Anthony, S., Vandergriff, A., de Andrade, J.B.M., Allen, T., Caranasos, T.G., Lobo, L.J., and Cheng, K. (2015). Adult lung spheroid cells contain progenitor cells and mediate regeneration in rodents with bleomycin-induced pulmonary fibrosis. Stem Cells Transl. Med. *4*, 1265–1274. https://doi.org/10.5966/sctm.2015-0062.

8. Cores, J., Hensley, M.T., Kinlaw, K., Rikard, S.M., Dinh, P.-U., Paudel, D., Tang, J., Vandergriff, A.C., Allen, T.A., Li, Y., et al. (2017). Safety and efficacy of allogeneic lung spheroid cells in a mismatched rat model of pulmonary fibrosis. Stem Cells Transl. Med. *6*, 1905–1916. https://doi.org/10.1002/sctm.16-0374.

9. Cores, J., Dinh, P.U.C., Hensley, T., Adler, K.B., Lobo, L.J., and Cheng, K. (2020). A pre-investigational new drug study of lung spheroid cell therapy for treating pulmonary fibrosis. Stem Cells Transl. Med. *9*, 786–798. https://doi.org/10.1002/sctm.19-0167.

10. Sengupta, V., Sengupta, S., Lazo, A., Woods, P., Nolan, A., and Bremer, N. (2020). Exosomes derived from bone marrow mesenchymal stem cells as treatment for severe COVID-19. Stem Cell. Dev. *29*, 747–754. https://doi.org/10.1089/scd.2020.0080.

11. Maremanda, K.P., Sundar, I.K., and Rahman, I. (2019). Protective role of mesenchymal stem cells and mesenchymal stem cell-derived exosomes in cigarette smoke-induced mitochondrial dysfunction in mice. Toxicol. Appl. Pharmacol. *385*, 114788. https://doi.org/10.1016/j.taap.2019.114788.

12. Mansouri, N., Willis, G.R., Fernandez-Gonzalez, A., Reis, M., Nassiri, S., Mitsialis, S.A., and Kourembanas, S. (2019). Mesenchymal stromal cell exosomes prevent and revert experimental pulmonary fibrosis through modulation of monocyte phenotypes. JCI Insight *4*, 128060. https://doi.org/10.1172/jci.insight.128060.

13. Dinh, P.-U.C., Paudel, D., Brochu, H., Popowski, K.D., Gracieux, M.C., Cores, J., Huang, K., Hensley, M.T., Harrell, E., Vandergriff, A.C., et al. (2020). Inhalation of lung spheroid cell secretome and exosomes promotes lung repair in pulmonary fibrosis. Nat. Commun. *11*, 1064. https://doi.org/10.1038/s41467-020-14344-7.

14. Zhang, N.-N., Li, X.-F., Deng, Y.-Q., Zhao, H., Huang, Y.-J., Yang, G., Huang, W.-J., Gao, P., Zhou, C., Zhang, R.-R., et al. (2020). A thermostable mRNA vaccine against COVID-19. Cell *182*, 1271–1283.e16. https://doi.org/10.1016/j.cell.2020.07.024.

15. Corbett, K.S., Edwards, D.K., Leist, S.R., Abiona, O.M., Boyoglu-Barnum, S., Gillespie, R.A., Himansu, S., Schäfer, A., Ziwawo, C.T., DiPiazza, A.T., et al. (2020). SARS-CoV-2 mRNA vaccine design enabled by prototype pathogen preparedness. Nature *586*, 567–571. https://doi.org/10.1038/s41586-020-2622-0.

16. Polack, F.P., Thomas, S.J., Kitchin, N., Absalon, J., Gurtman, A., Lockhart, S., Perez, J.L., Pérez Marc, G., Moreira, E.D., Zerbini, C., et al. (2020). Safety and efficacy of the BNT162b2 mRNA covid-19 vaccine. N. Engl. J. Med. *383*, 2603–2615. https://doi.org/10.1056/NEJMoa2034577.

17. Walsh, E.E., Frenck, R.W.J., Falsey, A.R., Kitchin, N., Absalon, J., Gurtman, A., Lockhart, S., Neuzil, K., Mulligan, M.J., Bailey, R., et al. (2020). Safety and immunogenicity of two RNA-based covid-19 vaccine candidates. N. Engl. J. Med. *383*, 2439–2450. https://doi.org/10.1056/NEJMoa2027906.

18. Wilkinson, T.M.A., Schembri, S., Brightling, C., Bakerly, N.D., Lewis, K., MacNee, W., Rombo, L., Hedner, J., Allen, M., Walker, P.P., et al. (2019). Non-typeable Haemophilus influenzae protein vaccine in adults with COPD: a phase 2 clinical trial. Vaccine *37*, 6102–6111. https://doi.org/10.1016/j.vaccine.2019.07.100.

19. Yang, J., Wang, W., Chen, Z., Lu, S., Yang, F., Bi, Z., Bao, L., Mo, F., Li, X., Huang, Y., et al. (2020).

A vaccine targeting the RBD of the S protein of SARS-CoV-2 induces protective immunity. Nature *586*, 572–577. https://doi.org/10.1038/s41586-020-2599-8.

20. Beija, M., Salvayre, R., Lauth-de Viguerie, N., and Marty, J.-D. (2012). Colloidal systems for drug delivery: from design to therapy. Trends Biotechnol. *30*, 485–496. https://doi.org/10.1016/j.tibtech.2012.04.008.

21. Sharma, J., Kalra, S., Sharma, A., and Rani, S. (2009). Colloidal drug carriers. Internet J. Fam. Pract. *9*.

22. Paranjpe, M., and Müller-Goymann, C. (2014). Nanoparticle-mediated pulmonary drug delivery: a review. Int. J. Mol. Sci. *15*, 5852–5873. https://doi.org/10.3390/ijms15045852.

23. Nanomedicine and the COVID-19 vaccines. Nat. Nanotechnol. *15*, 963. https://doi.org/10.1038/s41565-020-00820-0.

24. Radiom, M., Sarkis, M., Brookes, O., Oikonomou, E.K., Baeza-Squiban, A., and Berret, J.-F. (2020). Pulmonary surfactant inhibition of nanoparticle uptake by alveolar epithelial cells. Sci. Rep. *10*, 19436. https://doi.org/10.1038/s41598-020-76332-7.

25. Théry, C., Zitvogel, L., and Amigorena, S. (2002). Exosomes: composition, biogenesis and function. Nat. Rev. Immunol. *2*, 569–579. https://doi.org/10.1038/nri855.

26. Maas, S.L.N., Breakefield, X.O., and Weaver, A.M. (2017). Extracellular vesicles: unique intercellular delivery vehicles. Trends Cell Biol. *27*, 172–188. https://doi.org/10.1016/j.tcb.2016.11.003.

27. Sung, B.H., von Lersner, A., Guerrero, J., Krystofiak, E.S., Inman, D., Pelletier, R., Zijlstra, A., Ponik, S.M., and Weaver, A.M. (2020). A live cell reporter of exosome secretion and uptake reveals pathfinding behavior of migrating cells. Nat. Commun. *11*, 2092. https://doi.org/10.1038/s41467-020-15747-2.

28. van Niel, G., D'Angelo, G., and Raposo, G. (2018). Shedding light on the cell biology of extracellular vesicles. Nat. Rev. Mol. Cell Biol. *19*, 213–228. https://doi.org/10.1038/nrm.2017.125.

29. Kao, C.-Y., and Papoutsakis, E.T. (2019). Extracellular vesicles: exosomes, microparticles, their parts, and their targets to enable their biomanufacturing and clinical applications. Curr. Opin. Biotechnol. *60*, 89–98. https://doi.org/10.1016/J.COPBIO.2019.01.005.

30. Popowski, K., Lutz, H., Hu, S., George, A., Dinh, P.-U., and Cheng, K. (2020). Exosome therapeutics for lung regenerative medicine. J. Extracell. Vesicles *9*, 1785161. https://doi.org/10.1080/20013078.2020.1785161.

31. Popowski, K.D., Dinh, P.-U.C., George, A., Lutz, H., and Cheng, K. (2021). Exosome therapeutics for COVID-19 and respiratory viruses. View, 20200186. https://doi.org/10.1002/VIW.20200186.

32. Li, Z., Wang, Z., Dinh, P.-U.C., Zhu, D., Popowski, K.D., Lutz, H., Hu, S., Lewis, M.G., Cook, A., Andersen, H., et al. (2021). Cell-mimicking nanodecoys neutralize SARS-CoV-2 and mitigate lung injury in a non-human primate model of COVID-19. Nat. Nanotechnol. *16*, 942–951. https://doi.org/10.1038/s41565-021-00923-2.

33. Hutcheson, J.D., and Aikawa, E. (2018). Extracellular vesicles in cardiovascular homeostasis and disease. Curr. Opin. Cardiol. *33*, 290–297. https://doi.org/10.1097/HCO.0000000000000510.

34. Li, S.p., Lin, Z.x., Jiang, X., Yu, X.y., and Yu, X. (2018). Exosomal cargo-loading and synthetic exosome-mimics as potential therapeutic tools. Acta Pharmacol. Sin. *39*, 542–551. https://doi.org/10.1038/aps.2017.178.

35. Lutz, H., Popowski, K.D., Dinh, P.-U.C., and Cheng, K. (2021). Advanced nanobiomedical approaches to combat coronavirus disease of 2019. Adv. Nanobiomed Res. 2000063. https://doi.org/10.1002/anbr.202000063.

36. Kim, G.Y., Lee, Y., Ha, J., Han, S., and Lee, M. (2021). Engineering exosomes for pulmonary delivery of peptides and drugs to inflammatory lung cells by inhalation. J. Contr. Release *330*, 684–695. https://doi.org/10.1016/j.jconrel.2020.12.053.

37. Zhang, D., Lee, H., Wang, X., Rai, A., Groot, M., and Jin, Y. (2018). Exosome-Mediated small RNA delivery: a novel therapeutic approach for inflammatory lung responses. Mol. Ther. *26*, 2119–2130. https://doi.org/10.1016/j.ymthe.2018.06.007.

38. Wong, C., West, P.E., Olson, K.S., Mecartney, M.L., and Starostina, N. (2007). Tip dilation and AFM capabilities in the characterization of nanoparticles. JOM *59*, 12–16. https://doi.org/10.1007/s11837-007-0003-x.

39. Eaton, P., Quaresma, P., Soares, C., Neves, C., de Almeida, M.P., Pereira, E., and West, P. (2017). A direct comparison of experimental methods to measure dimensions of synthetic nanoparticles. Ultramicroscopy *182*, 179–190. https://doi.org/10.1016/j.ultramic.2017.07.001.

40. Fennelly, K.P. (2020). Particle sizes of infectious aerosols: implications for infection control. Lancet Respir. Med. *8*, 914–924. https://doi.org/10.1016/S2213-2600(20)30323-4.

41. Kretschmer, S., Pieper, M., Hüttmann, G., Bölke, T., Wollenberg, B., Marsh, L.M., Garn, H., and König, P. (2016). Autofluorescence multiphoton microscopy for visualization of tissue morphology and cellular dynamics in murine and human airways. Lab. Invest. *96*, 918–931. https://doi.org/10.1038/labinvest.2016.69.

42. Davis, A.S., Richter, A., Becker, S., Moyer, J.E., Sandouk, A., Skinner, J., and Taubenberger, J.K. (2014). Characterizing and diminishing autofluorescence in formalin-fixed paraffin-embedded human respiratory tissue. J. Histochem. Cytochem. *62*, 405–423. https://doi.org/10.1369/0022155414531549.

43. Zhou, X., Xie, F., Wang, L., Zhang, L., Zhang, S., Fang, M., and Zhou, F. (2020). The function and clinical application of extracellular vesicles in innate immune regulation. Cell. Mol. Immunol. *17*, 323–334. https://doi.org/10.1038/s41423-020-0391-1.

44. Twigg, H.L., 3rd. (2005). Humoral immune defense (antibodies): recent advances. Proc. Am. Thorac. Soc. *2*, 417–421. https://doi.org/10.1513/pats.200508-089JS.

45. Dinh, P.-U.C., Cores, J., Hensley, M.T., Vandergriff, A.C., Tang, J., Allen, T.A., Caranasos, T.G., Adler, K.B., Lobo, L.J., and Cheng, K. (2017). Derivation of therapeutic lung spheroid cells from minimally invasive transbronchial pulmonary biopsies. Respir. Res. *18*, 132. https://doi.org/10.1186/s12931-017-0611-0.

46. Greening, D.W., Xu, R., Ji, H., Tauro, B.J., and Simpson, R.J. (2015). A protocol for exosome isolation and characterization: evaluation of ultracentrifugation, density-gradient separation, and immunoaffinity capture methods. Methods Mol. Biol. *1295*, 179–209. https://doi.org/10.1007/978-1-4939-2550-6_15.

47. Bosch, S., de Beaurepaire, L., Allard, M., Mosser, M., Heichette, C., Chrétien, D., Jegou, D., and Bach, J.-M. (2016). Trehalose prevents aggregation of exosomes and cryodamage. Sci. Rep. *6*, 36162. https://doi.org/10.1038/srep36162.

48. Naseri, Z., Oskuee, R.K., Jaafari, M.R., and Forouzandeh Moghadam, M. (2018). Exosome-mediated delivery of functionally active miRNA-142-3p inhibitor reduces tumorigenicity of breast cancer in vitro and in vivo. Int. J. Nanomed. *13*, 7727–7747. https://doi.org/10.2147/IJN.S182384.

49. Abdelwahed, W., Degobert, G., Stainmesse, S., and Fessi, H. (2006). Freeze-drying of nanoparticles: formulation, process and storage considerations. Adv. Drug Deliv. Rev. *58*, 1688–1713. https://doi.org/10.1016/j.addr.2006.09.017.

Matter, Volume *5*

Supplemental information

Inhalable dry powder mRNA vaccines based on extracellular vesicles

Kristen D. Popowski, Adele Moatti, Grant Scull, Dylan Silkstone, Halle Lutz, Blanca López de Juan Abad, Arianna George, Elizabeth Belcher, Dashuai Zhu, Xuan Mei, Xiao Cheng, Megan Cislo, Asma Ghodsi, Yuheng Cai, Ke Huang, Junlang Li, Ashley C. Brown, Alon Greenbaum, Phuong-Uyen C. Dinh, and Ke Cheng

Supplementary Materials

SUPPLEMENTARY METHODS

SDS-PAGE and western blot

Samples were lysed, denatured, and reduced by Laemmli sample buffer (Bio-Rad, Hercules, CA, USA) and β-mercaptoethanol (Bio-Rad, Hercules, CA, USA) at 90°C for 5 minutes. Protein samples and molecular ladder (Precision Plus Protein Unstained Standards; Bio-Rad, Hercules, CA, USA) were loaded into a 10% acrylamide precast Tris-Glycine gel (Bio-Rad, Hercules, CA, USA) for sodium dodecyl sulfate polyacrylamide gel electrophoresis (SDS-PAGE) separation. Gels were run at a stacking voltage of 100V until samples ran out of the wells, followed by a constant voltage of 200V. Gels were visualized and imaged in a Bio-Rad Imager (Bio-Rad, Hercules, CA, USA). Gels were transferred onto polyvinylidene fluoride membranes (PVDF; Bio-Rad, Hercules, CA, USA) using the Bio-Rad wet electroblotting transfer system (Bio-Rad, Hercules, CA, USA). Following transfer, membranes were washed three times in 1X phosphate-buffered saline with 0.1% Tween detergent (PBS-T; MilliporeSigma, Burlington, MA, USA) for 5 minutes each and blocked using 5% milk in PBS-T for one hour at room temperature. Membranes were blotted against anti-β-Actin (ab6276; Abcam, Cambridge, United Kingdom), anti-RFP (ab62341; Abcam, Cambridge, United Kingdom), and anti-Spike (40592-T62; Sino Biological, Beijing, China) primary antibodies in 5% milk in PBS-T and incubated at 4°C for one week. After incubation, membranes were incubated with the corresponding goat anti-rabbit (ab6721; Abcam, Cambridge, United Kingdom) and goat anti-mouse (ab6789; Abcam, Cambridge, United Kingdom) HRP-conjugated secondary antibodies for 1 hour at room temperature. Membranes were then visualized using Clarity Western ECL Substrate (Bio-Rad,

Hercules, CA, USA) and imaged in a Bio-Rad Imager (Bio-Rad, Hercules, CA, USA). Band intensities were analyzed using ImageJ analysis software (NIH; https://imagej.nih.gov/ij/).

Tissue clearing and imaging

Mouse lungs were cleared using the BoneClear protocol.[S1,S2] Anesthetized mice were perfused with DPBS and 50 μg/mL heparin (Sigma-Aldrich, St. Louis, MO, USA). Lung tissues were dissected and fixed in a DPBS, 0.5% PFA (Electron Microscopy Sciences, Hatfield, PA, USA), and 10% sucrose (Sigma-Aldrich, St. Louis, MO, USA) solution at room temperature, then further fixed overnight in a DPBS and 0.5% PFA solution at 4°C. Fixed lung samples were incubated in a methanol (VWR, Randor, PA, USA) gradient of 20%, 40%, 60%, 80%, and 100% for two hours per percentage at room temperature. Then, the samples were decolorized overnight in a 30% hydrogen peroxide (Sigma-Aldrich, St. Louis, MO, USA) and 100% methanol solution at a 1:10 ratio respectively at 4°C. Lung tissues were then incubated in a reverse methanol gradient at room temperature and permeabilized with a DPBS, 0.02% Triton X-100 (Sigma-Aldrich, St. Louis, MO, USA), 0.01% sodium deoxycholate (Sigma-Aldrich, St. Louis, MO, USA), 10% dimethyl sulfoxide (DMSO; Sigma-Aldrich, St. Louis, MO, USA), 25 mM EDTA (Sigma-Aldrich, St. Louis, MO, USA) solution at 37°C overnight. Lung samples were then blocked with a DPBS, 0.02% Triton X-100, 10% DMSO, 5% normal donkey serum (Sigma-Aldrich, St. Louis, MO, USA), and 25 mM EDTA solution overnight at 37°C. Lung tissues were immunolabeled with anti-RFP (ab62341; Abcam, Cambridge, United Kingdom) primary antibody diluted in a DPBS, 0.02% Tween-20, 1 g/mL heparin, 5% normal donkey serum, and 25 mM EDTA solution at a 1:200 ratio respectively for one week at 37°C. Tissues were washed and further immunolabeled with Cy3 (711-165-152; Jackson ImmunoResearch Laboratories, West Grove, PA, USA) secondary antibody diluted in a DBPS, 0.02% Tween-20, 1 g/mL

heparin, 5% normal donkey serum, and 25 mM EDTA solution at a 1:500 ratio respectively for 5 days at 37°C. Lung tissues were washed, incubated in a methanol gradient, then incubated twice in a dichloromethane (Sigma-Aldrich, St. Louis, MO, USA) and methanol solution at a 1:2 ratio respectively at room temperature, and followed by four incubations in 100% dichloromethane. Finally, lung samples were cleared three times with 100% dibenzyl-ether (Sigma-Aldrich, St. Louis, MO, USA) at room temperature and imaged using a custom-built light sheet microscope.[S1] Whole lung images and movies were captured using Imaris image analysis software (Imaris, Oxford Instruments, Abingdon, United Kingdom).

Particle segmentation

Cleared mouse lungs were analyzed using ImageJ analysis software. In each image, pixels that belonged to exosomes or liposomes were segmented via thresholding, during which the intensity threshold was decided manually. The selection brush tool was used to refine the masks generated by thresholding and to segment the airway regions. Quantification of areas or pixels was then performed based on the extracted masks.

Flow cytometry

Exosome and liposome uptake were evaluated in lung parenchymal cells and single-cell suspensions of murine lung cells by flow cytometry. Lung parenchymal cells were co-cultured with RFP-Exo and RFP-Lipo for 24 hours to evaluate nanoparticle protein cargo uptake. Lung parenchymal cells were co-cultured with RFP-Exo and RFP-Lipo for 1 minute to evaluate nanoparticle mRNA cargo uptake. Single-cell suspensions of murine lung cells were generated from mice that received nebulized RFP-Exo or RFP-Lipo. Lung parenchymal cells and murine lung cells were permeabilized (BD, Franklin Lakes, NJ, USA), GFP (ab290; Abcam, Cambridge, United Kingdom) and RFP primary antibodies were incubated for 1 hour at 4°C, and their

corresponding goat anti-rabbit AF488-conjugated (ab150077; Abcam, Cambridge, United Kingdom) and AF647-conjugated (ab150079; Abcam, Cambridge, United Kingdom) secondary antibodies were incubated for 1 hour at 4°C. The internalization of nanoparticle mRNA and protein cargo by cells was examined by flow cytometry (CytoFlex, Beckman Coulter, Brea, CA, USA).

Air-liquid interface system

A model of the human airway at the air-liquid interface was created by seeding human bronchial epithelial cells onto a 0.4 μm pore polycarbonate membrane and lung parenchymal cells onto a 6.5 mm well in a transwell system (Corning Incorporated, Corning, NY, USA). Cells were maintained for one week before administering DiD-labeled exosomes and liposomes to the human bronchial epithelial cells. Nuclei in the transwell wells were visualized by adding NucBlue™ Live ReadyProbes™ Reagent (R37605; ThermoFisher Scientific, Waltham, MA, USA) to the media and analyzed using ImageJ analysis software.

DPI fabrication

A DPI for nanoparticle inhalation to mice was fabricated as previously described, with modifications.[S3] The inhalation apparatus was adapted by using a plastic microcentrifuge tube as the powder receptacle. A plastic 250 mL centrifuge tube was attached to the powder receptacle to serve as a containment chamber for the un-anesthetized mouse; this optimized mouse muzzle orientation. A DPI for nanoparticle inhalation to primates was assembled using the RS01 high-resistance DPI (239700002AA; Berry Global, Evansville, IN, USA) connected to an aerosol chamber inhaler spacer (Canack Technology Ltd., Vancouver, Canada).

Histology

Immunostaining was performed on transwell membranes and tissue slides fixed in 4% PFA (Electron Microscopy Sciences, Hatfield, PA, USA) in DPBS for 30 minutes, followed by permeabilization and blocking with Dako Protein blocking solution (Aglient Technologies, Santa Clara, CA, USA) with 0.1% saponin (Sigma-Aldrich, St. Louis, MO, USA) at room temperature for 1 hour. Membranes were immunolabeled with anti-MUC5b (ab77995; Abcam, Cambridge, United Kingdom) primary antibody diluted in Dako Protein blocking solution and its corresponding goat anti-mouse (A10667; Invitrogen, Waltham, MA, USA) AF488-conjugated secondary antibody diluted in Dako Protein blocking solution. Membranes and slides were mounted with ProLong Gold Antifade Mountant (Invitrogen, Waltham, MA, USA) and ProLong Gold Antifade Mountant with DAPI (Invitrogen, Waltham, MA, USA). Membrane and slides were imaged on the Olympus FLUOVIEW CLSM (Olympus; FV3000, Shinjuku, Tokyo, Japan) with an Olympus UPlanSAPO 10x objective (Olympus; 1-U2B824, Shinjuku, Tokyo, Japan) and Olympus UPlanSAPO 60x objective (Olympus; 1-U2B832, Shinjuku, Tokyo, Japan). H&E staining was performed on tissue slides (Hematoxylin HHS16; Eosin 318906; Sigma-Aldrich, St. Louis, MO, USA) and imaged on the Leica DMi8 (Leica Microsystems, Wetzlar, Germany). Tissue slides were analyzed using ImageJ analysis software.

AFM imaging

Lung-Exo, HEK-Exo, and Lipo were prepared as freshly isolated particles in PBS and trehalose solution (Fresh), lyophilized powder (Lyophilized), and lyophilized powder reconstituted in DNase/RNase-free distilled water (Invitrogen, Waltham, MA, USA) (Reconstituted). Samples were added onto coverslips functionalized by (3-Aminopropyl)triethoxysilane (APTMS; Sigma-Aldrich, St. Louis, MO, USA) as previously described.[S4,S5] Samples were imaged on the MFP-3D AFM (Asylum Research, Oxford Instruments, Abingdon, United Kingdom) with a silicon

scanning probe microscopy-sensor probe (ARROW-NCR-50; Neuchâtel, Switzerland). Height and diameter measurements were analyzed using Asylum Research Software Version 16 (Asylum Research, Oxford Instruments, Abingdon, United Kingdom) ran on Igor Pro 6 (WaveMetrics, Tigard, OR, USA).

Particle counting

Lyophilized Lung-Exo, HEK-Exo, and Lipo were encapsulated in Quali V Inhalation capsules (Qualicaps, Inc., Whitsett, NC, USA) and inserted into low-, medium-, high-, and ultra-high-resistance DPIs (Berry Global, Evansville, IN, USA). The DPIs were inserted into a negative-pressure vacuum chamber to aerosolize the samples. Samples were aerosolized for 30 seconds, followed by particle size distribution measurement using the TSI AeroTrak particle counter (9306-V2, TSI, Shoreview, MN, USA) for 1-minute time intervals at ambient room temperature. Differential particle counts measure values ranging from one bin size (i.e. 3 µm) up to, but not including, its successive bin size (i.e. 5 µm). Cumulative particle counts measure values from one bin size (i.e. 3 µm) and greater. Bin sizes within the respirable fraction and nanoparticle biodistribution[S6] in the lung determined the optimal resistance DPI.

SUPPLEMENTARY FIGURES

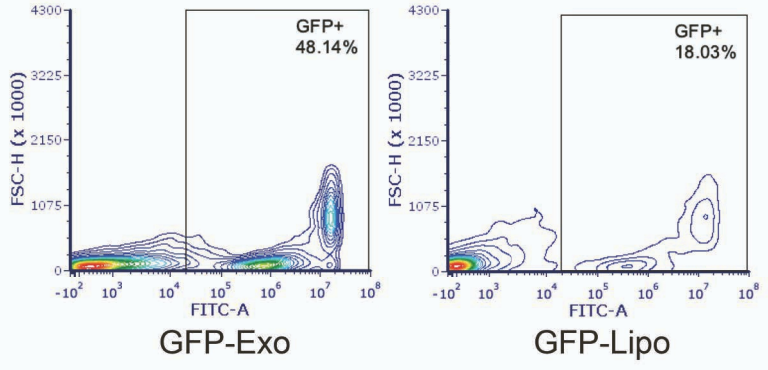

Fig. S1. mRNA uptake by lung parenchymal cells. Flow cytometry analysis of lung parenchymal cells co-cultured with GFP-Exo or GFP-Lipo.

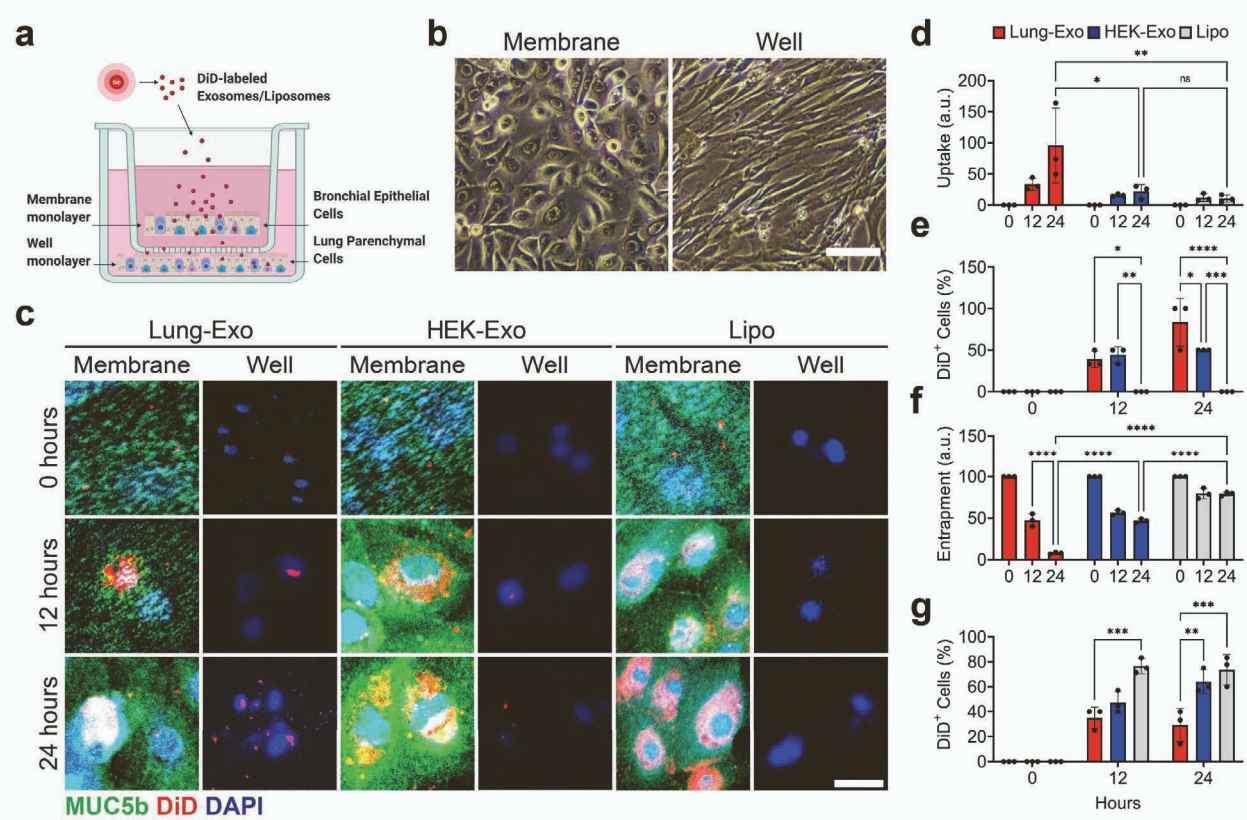

Fig. S2. Mucus penetrance of nanoparticles. (A) Schematic of DiD labeling and administration to an air-liquid interface transwell system. Created with BioRender.com. (B) Brightfield images of human bronchial epithelial cells on the transwell membrane and lung parenchymal cells on the transwell well; scale bar=10 μm. (C) Representative immunostaining images of transwell membranes and transwell wells for MUC5b (green), DiD (red), and DAPI (blue); scale bar=10 μm. (D) Quantification of Lung-Exo, HEK-Exo, and Lipo pixel intensity normalized to nuclei in lung parenchymal cells; n=3 per group. (E) Percentage of DiD^+ lung parenchymal cells; n=3 per group. (F) Quantification of Lung-Exo, HEK-Exo, and Lipo pixel intensity normalized to nuclei

in human bronchial epithelial cells; n=3 per group. (G) Percentage of DiD^+ human bronchial epithelial cells; n=3 per group.

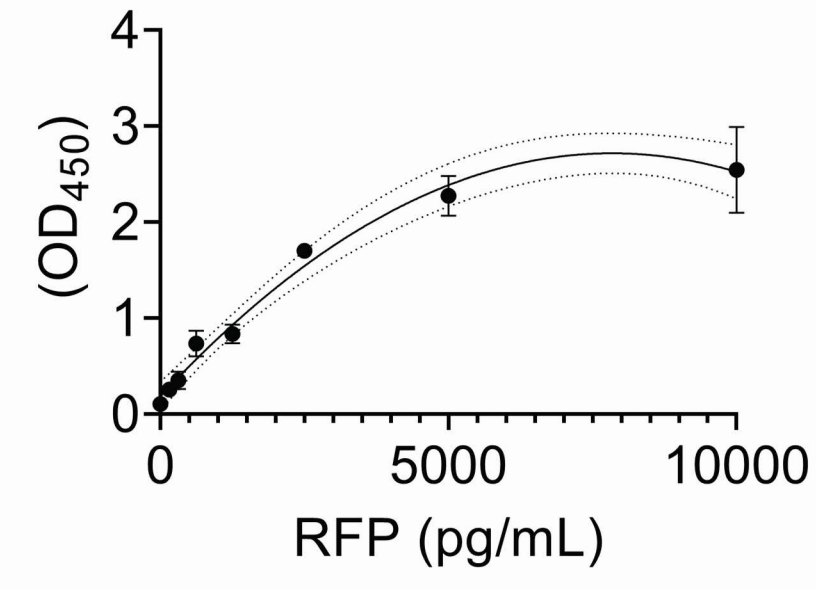

Fig. S3. Standard curve for cargo leakage. Standard curve of RFP concentrations in duplicates. Interpolation of the standard curve is represented by the solid line. The 95% confidence interval is represented by the dashed line.

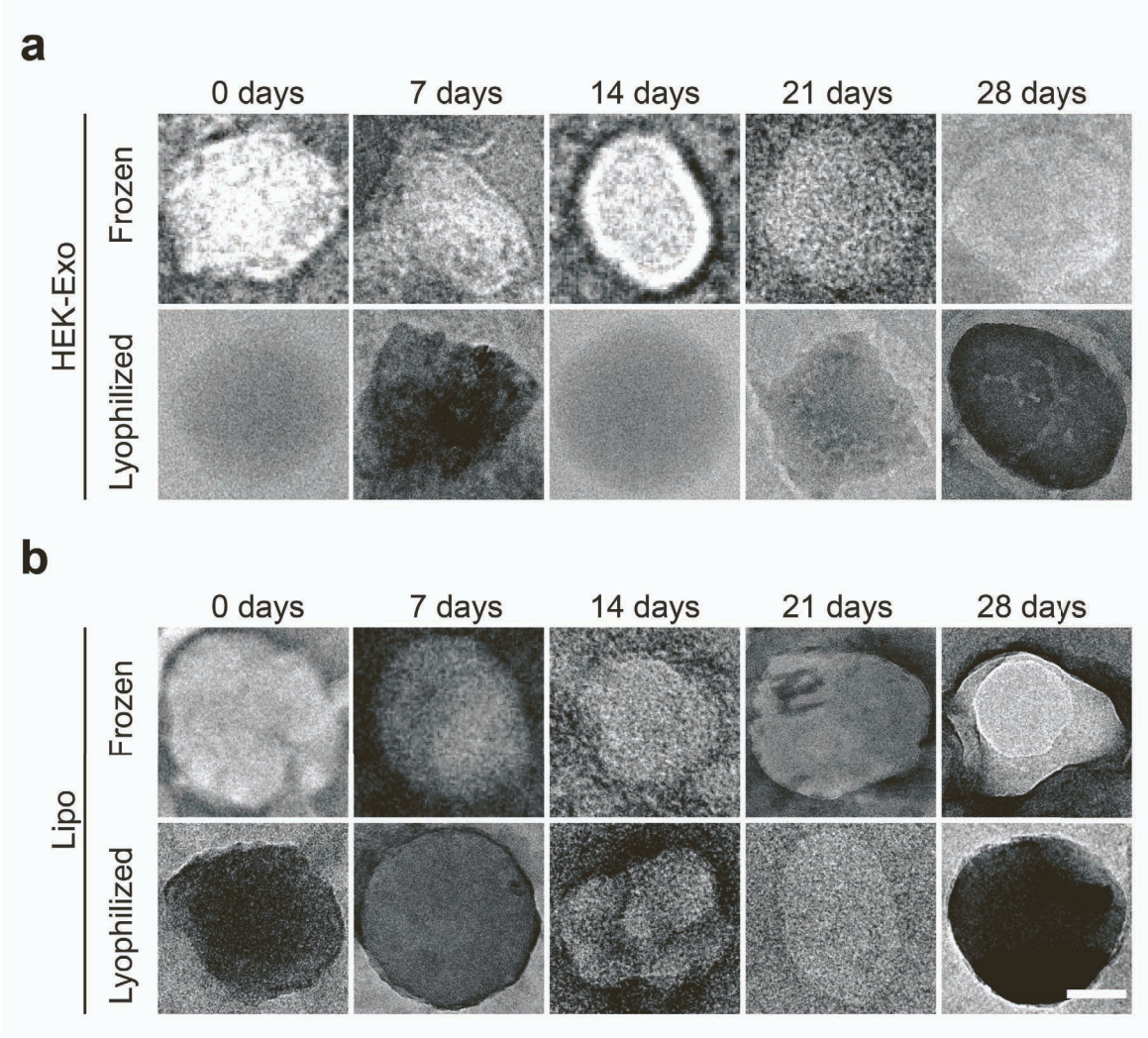

148

149 **Fig. S4. Morphology of nanoparticles at fresh and lyophilized formulations.** TEM images of

150 HEK-Exo (A) and Lipo (B) at frozen (Frozen) or room (Lyophilized) temperatures; scale bar=50

151 nm.

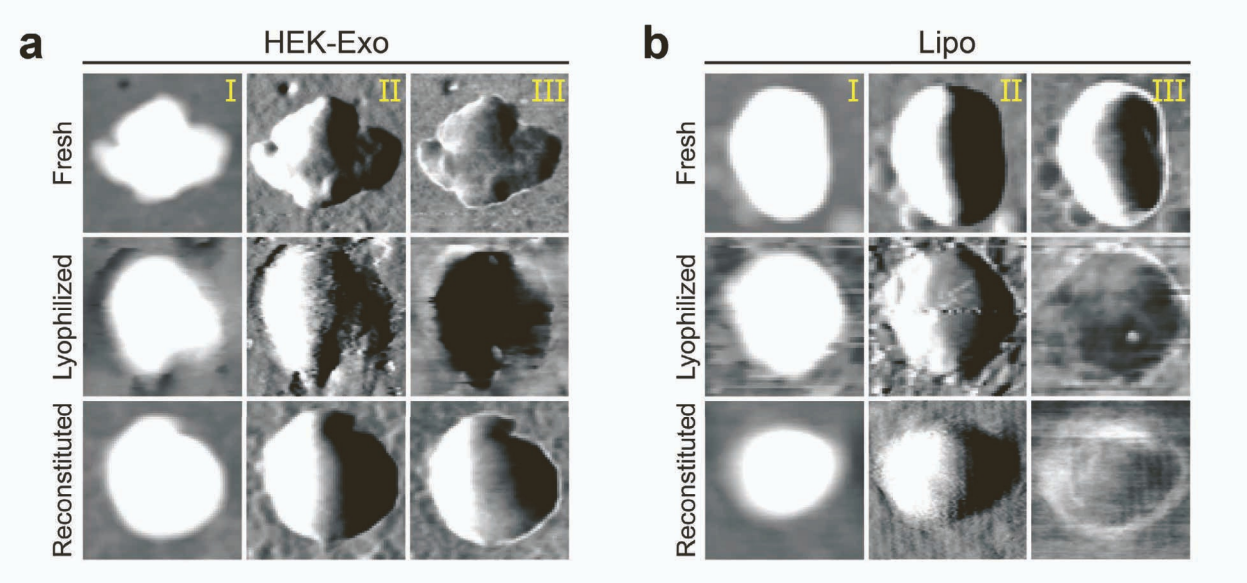

Fig. S5. Membrane integrity of nanoparticles across formulations. Representative AFM height (i), amplitude (ii), and phase (iii) images of HEK-Exo (A) and Lipo (B) across fresh, lyophilized, and reconstituted formulations.

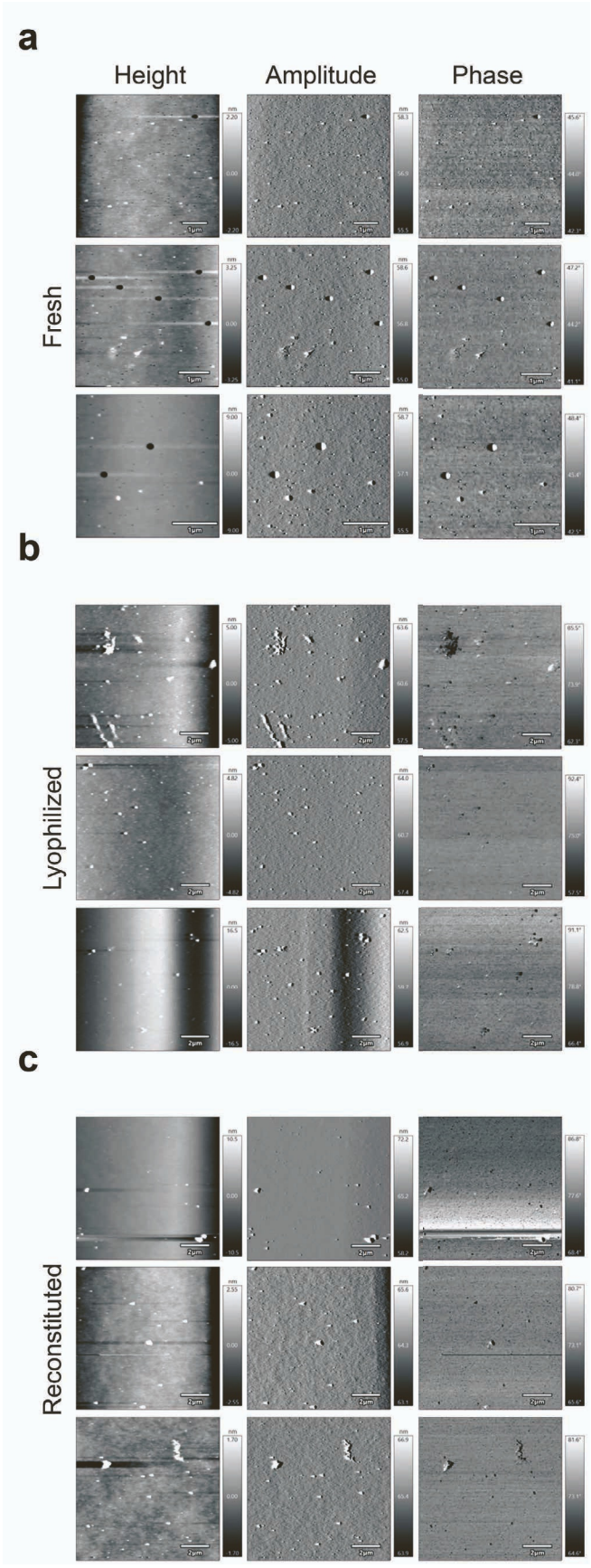
a
Height
Amplitude
Phase
Fresh
b
Lyophilized
c
Reconstituted

156

Fig. S6. Clumping properties of Lung-Exo. AFM images of fresh (A), lyophilized (B) and reconstituted (C) Lung-Exo across fresh, lyophilized, and reconstituted formulations.

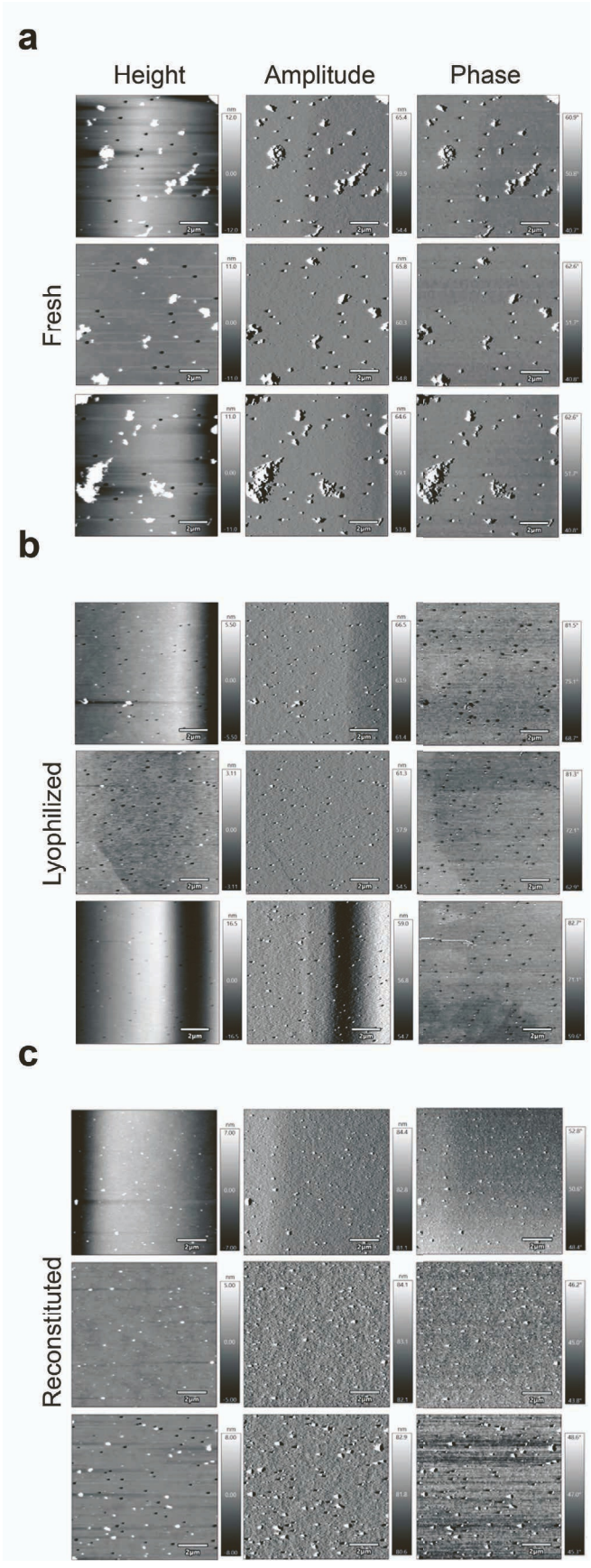
a
Height
Amplitude
Phase
Fresh
b
Lyophilized
c
Reconstituted

159

Fig. S7. Clumping properties of HEK-Exo. AFM images of fresh (A), lyophilized (B) and reconstituted (C) HEK-Exo across fresh, lyophilized, and reconstituted formulations.

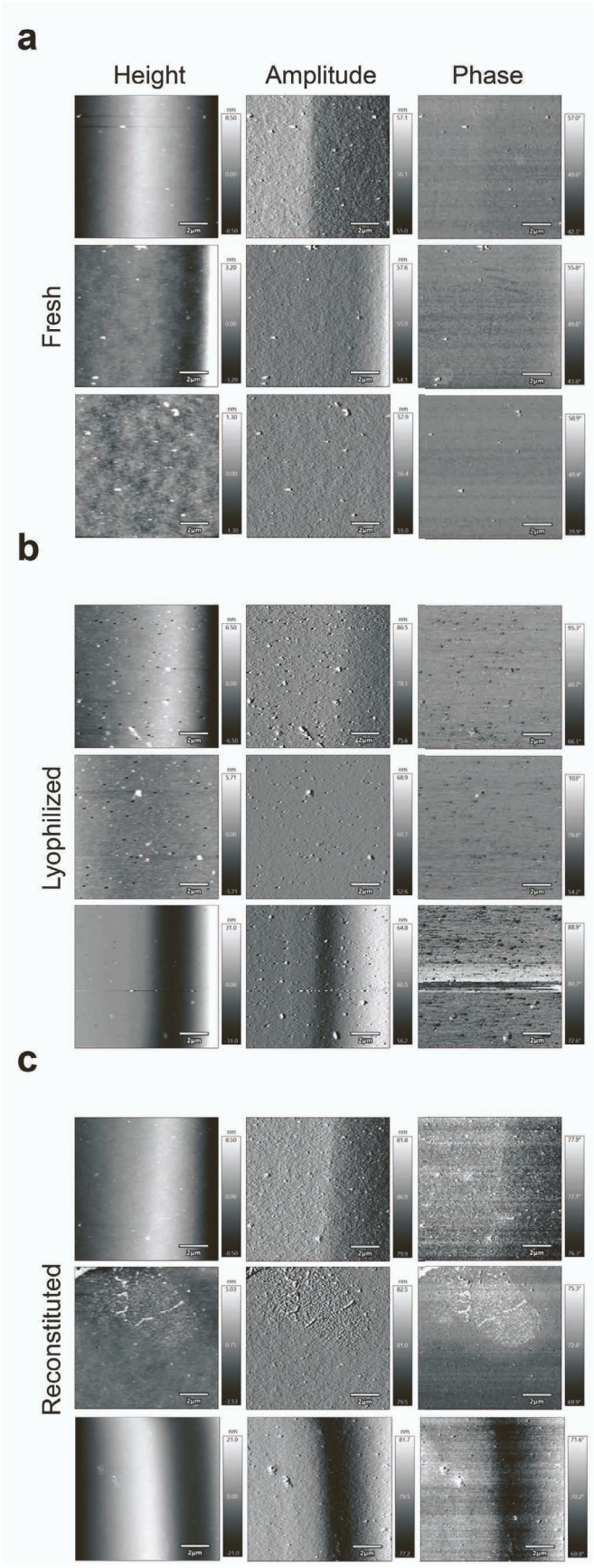
a
Height
Amplitude
Phase
Fresh
b
Lyophilized
c
Reconstituted

Fig. S8. Clumping properties of Lipo. AFM images of fresh (A), lyophilized (B) and reconstituted (C) Lipo across fresh, lyophilized, and reconstituted formulations.

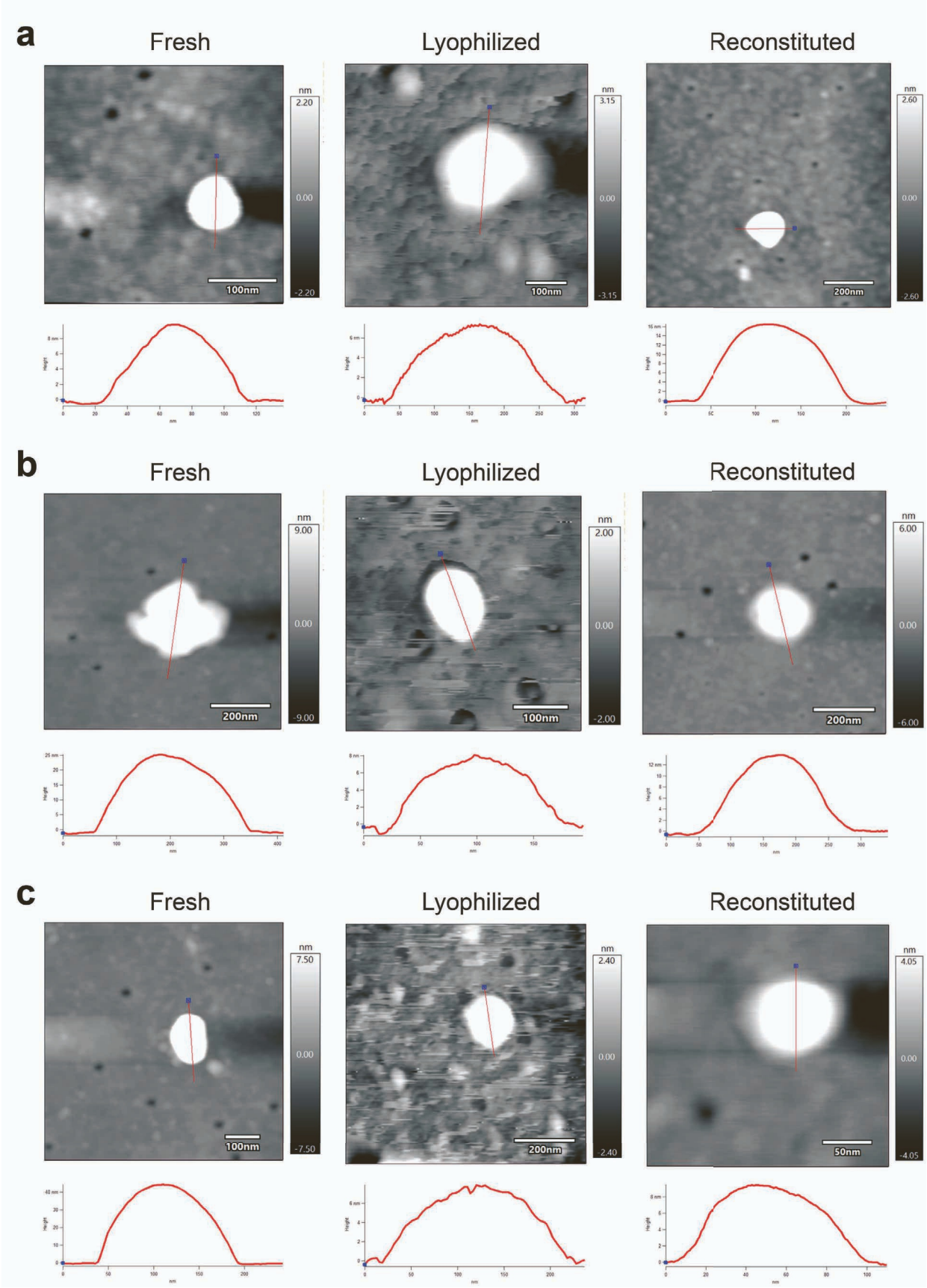
a
Fresh
Lyophilized
Reconstituted
nm
2.20
0.00
-2.20
100nm
nm
3.15
0.00
-3.15
100nm
nm
2.60
0.00
-2.60
200nm
b
Fresh
Lyophilized
Reconstituted
nm
9.00
0.00
-9.00
200nm
nm
2.00
0.00
-2.00
100nm
nm
6.00
0.00
-6.00
200nm
c
Fresh
Lyophilized
Reconstituted
nm
7.50
0.00
-7.50
100nm
nm
2.40
0.00
-2.40
200nm
nm
4.05
0.00
-4.05
50nm

165

Fig. S9. Cross-section measurements of nanoparticles. Representative AFM height images of Lung-Exo (A), HEK-Exo (B), and Lipo (C) across fresh, lyophilized, and reconstituted formulations. Cross-section measurements were repeated on nine singular Lung-Exo (see Fig. 2C), HEK-Exo (see Fig. S4), and Lipo (see Fig. S4) height images to obtain height and diameter measurements (see Fig. 2D).

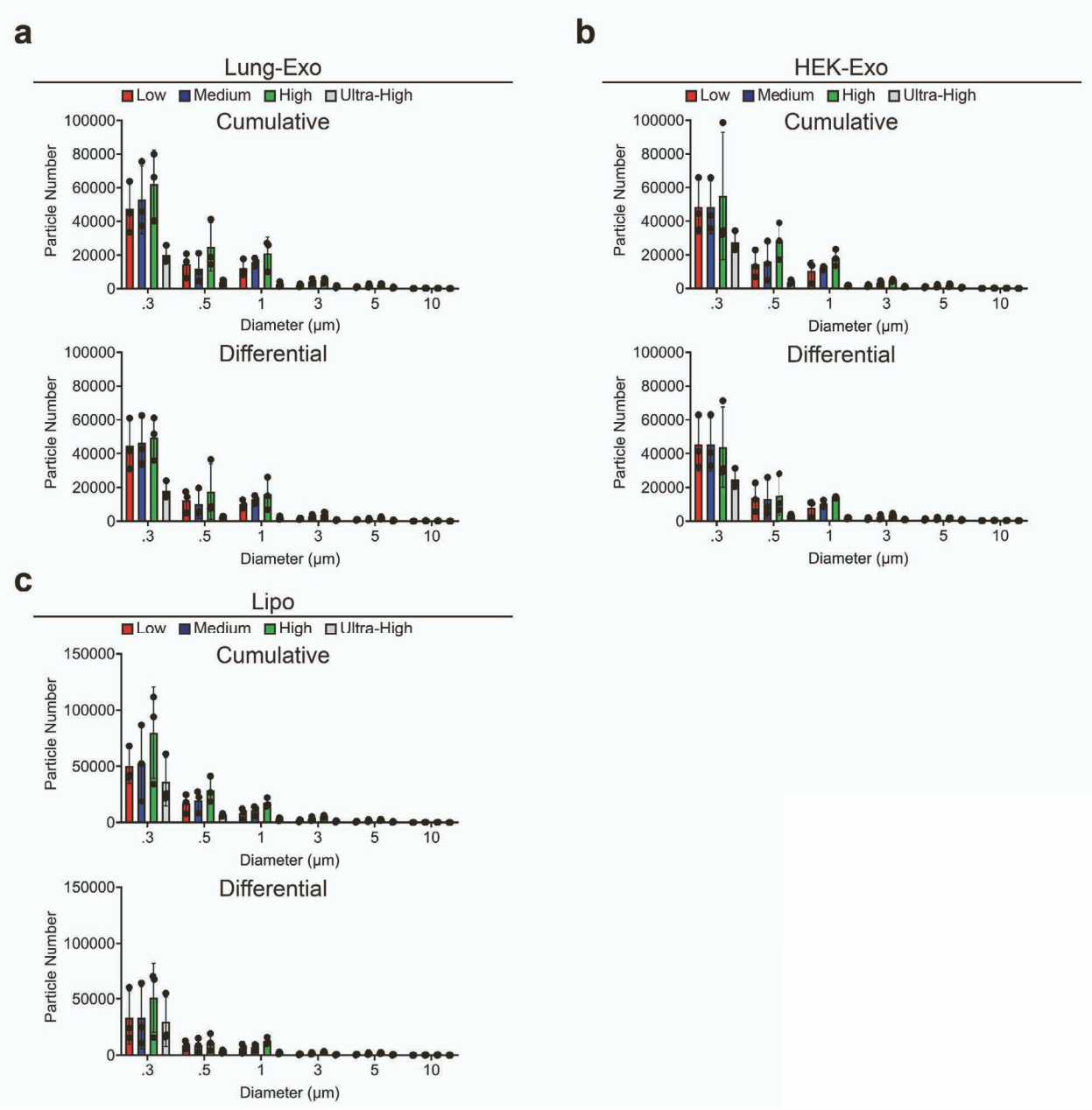

Fig. S10. Total particle counts from various resistance DPIs. Total cumulative and differential particle counts of Lung-Exo (A), HEK-Exo (B), and Lipo (C) distributed by low-, medium-, high-, and ultra-high-resistance DPIs.

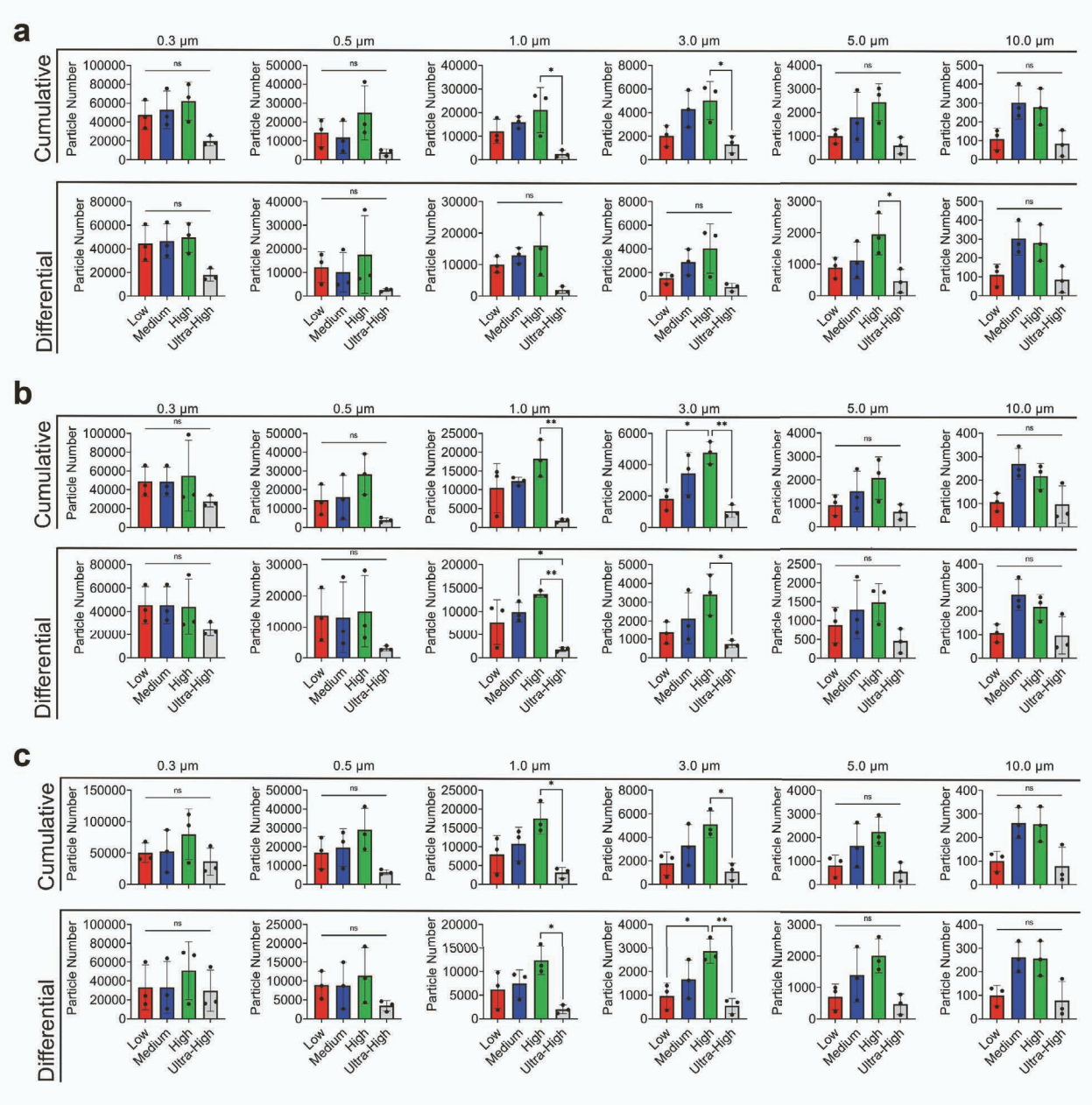

Fig. S11. Particle counts at six bin sizes from various resistance DPIs. Cumulative and differential particle count evaluation of LSC-Exo (A), HEK-Exo (B) and Lipo (C) distributed by low-, medium-, high-, and ultra-high-resistance DPI.

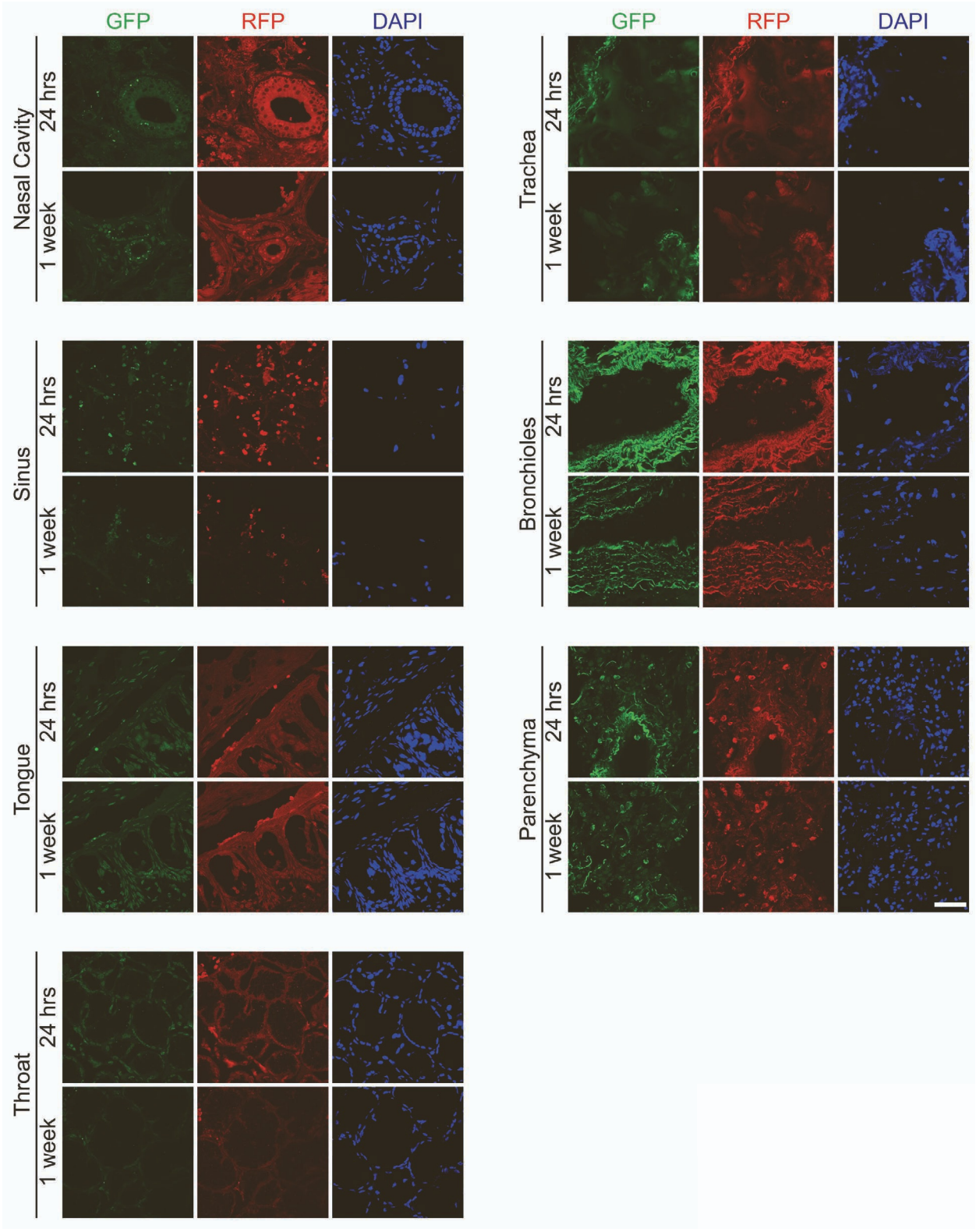
GFP
RFP
DAPI
Nasal Cavity
Trachea
Sinus
Bronchioles
Tongue
Parenchyma
Throat
1 week
24 hrs

179

Fig. S12. Immunostaining of simian upper and lower respiratory tracts. Representative split-channel immunostaining images of the following sections from AGMs that received Lung-Exo via DPI: nasal cavity, sinus, tongue, throat, trachea, bronchioles, and parenchyma sections for GFP (green), RFP (red) and DAPI (blue); scale bar=100 μm.

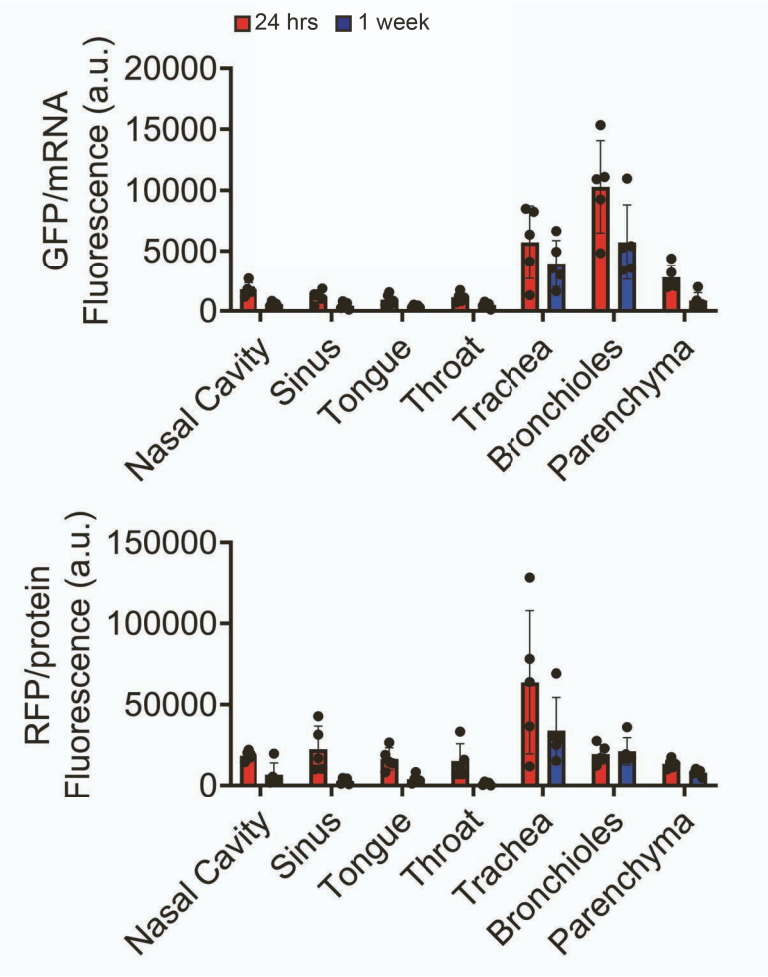

Fig. S13. Total exosome deposition in the simian upper and lower respiratory tracts. Quantification of mRNA and protein fluorescence in simian upper and lower respiratory tissues 24 hours and 1 week after lyophilized Lung-Exo via dry-powder inhalation.

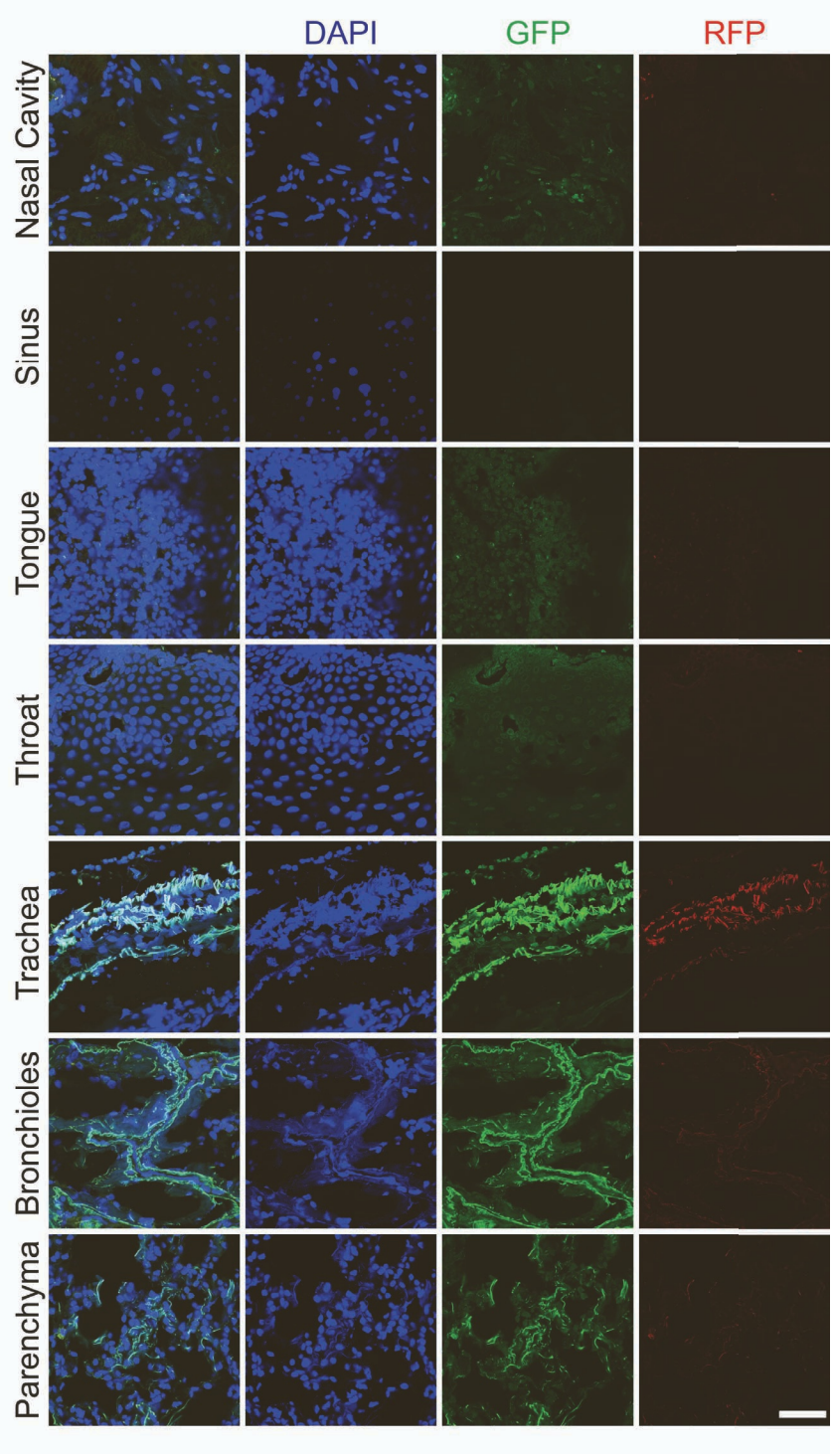

188

189 **Fig. S14. Autofluorescence of simian tissues.** Representative autofluorescence of the following

190 sections from AGMs that received no treatment: nasal cavity, sinus, tongue, throat, trachea,

191 bronchioles, and parenchyma sections for GFP (green) channel, RFP (red) channel, and DAPI

192 (blue) staining; scale bar=100 μm.

SUPPLEMENTAL REFERENCES

S1. Moatti A., Cai Y., Li C., Sattler T., Edwards L., Piedrahita J., et al. Three-dimensional imaging of intact porcine cochlea using tissue clearing and custom-built light-sheet microscopy. Biomed. Opt Express 2020;11:6181–6196. doi:10.1364/BOE.402991.

S2. Wang Q., Liu K., Yang L., Wang H., Yang J. BoneClear: whole-tissue immunolabeling of the intact mouse bones for 3D imaging of neural anatomy and pathology. Cell Res. 2019;29:870–872. doi:10.1038/s41422-019-0217-9.

S3. Kaur J., Muttil P., Verma R.K., Kumar K., Yadav A.B., Sharma R., et al. A hand-held apparatus for "nose-only" exposure of mice to inhalable microparticles as a dry powder inhalation targeting lung and airway macrophages. Eur. J. Pharmaceut. Sci. 2008;34:56–65. doi:10.1016/j.ejps.2008.02.008.

S4. Sproul E.P., Nandi S., Roosa C., Schreck L., Brown A.C. Biomimetic microgels with controllable deformability improve healing outcomes. Adv. Biosyst. 2018;2:1800042. doi:10.1002/adbi.201800042.

S5. Sproul E.P., Nandi S., Chee E., Sivadanam S., Igo B.J., Schreck L., et al. Development of biomimetic antimicrobial platelet-like particles comprised of microgel nanogold composites. Regen. Eng. Transl. Med. 2020;6:299–309. doi:10.1007/s40883-019-00121-6.

S6. Popowski Kristen, et al. Inhalable exosomes outperform liposomes as mRNA and protein drug carriers to the lung.. Extracellular Vesicle 2022. doi:https://doi.org/https://doi.org/10.1016/j.vesic.2022.100002.